View metadata, citation and similar papers at core.ac.uk

brought to you by CORE

provided by Carolina Digital Repository

HHS Public Access

Author manuscript

Eur J Neurosci. Author manuscript; available in PMC 2017 January 04.

Published in final edited form as:

Eur J Neurosci. 2016 January ; 43(2): 230–244. doi:10.1111/ejn.13116.

Structural and Functional Connectivity between the Lateral Posterior-Pulvinar Complex and Primary Visual Cortex in the Ferret

Chunxiu Yu[1], **Kristin K. Sellers**[1,2], **Susanne Radtke-Schuller**[1], **Jinghao Lu**[1], **Lei Xing**[5], **Vladimir Ghukasyan**[5], **Yuhui Li**[1], **Yen-Yu Ian Shih**[2,4,7,8], **Richard Murrow**[6,7], and **Flavio Frohlich**[1,2,3,4,5,7]

[1]Department of Psychiatry, University of North Carolina at Chapel Hill, Chapel Hill NC 27599

[2]Neurobiology Curriculum, University of North Carolina at Chapel Hill, Chapel Hill NC 27599

[3]Department of Cell Biology and Physiology, University of North Carolina at Chapel Hill, Chapel Hill NC 27599

[4]Department of Biomedical Engineering, University of North Carolina at Chapel Hill, Chapel Hill NC 27599

[5]Neuroscience Center, University of North Carolina at Chapel Hill, Chapel Hill NC 27599

[6]Department of Neurosurgery, University of North Carolina at Chapel Hill, Chapel Hill NC 27599

[7]Department of Neurology, University of North Carolina at Chapel Hill, Chapel Hill NC 27599

[8]Biomedical Research Imaging Center, University of North Carolina at Chapel Hill, Chapel Hill NC 27599

Abstract

The role of higher-order thalamic structures in sensory processing remains poorly understood. Here, we used the ferret (*Mustela putorius furo*) as a novel model species for the study of the lateral posterior-pulvinar complex (LP/pulvinar) and its structural and functional connectivity with area 17 (primary visual cortex, V1). We found reciprocal anatomical connections between the lateral part of the Lateral Posterior Nucleus of the LP/pulvinar (LPl) and V1. In order to investigate the role of this feedback loop between LPl and V1 in shaping network activity, we determined the functional interactions between LPl and supragranular, granular, and infragranular layers of V1 by recording multiunit activity (MUA) and local field potential (LFP). Coherence was strongest between LPl and supragranular V1 with the most distinct peaks in the delta and alpha frequency bands. Inter-area interaction measured by spike-phase coupling identified the

Correspondence should be addressed to: Flavio Frohlich, 115 Mason Farm Rd. NRB 4109F, Chapel Hill, NC. 27599. flavio_frohlich@med.unc.edu. Phone: 919.966.4584.

Authorship Statement: CY, KS, RM, and FF designed the experiments, CY and KS performed the experiments, YS performed the MR study, CY, SR, JL, YL and FF analyzed the data, CY, LX and VG performed the confocal imaging, and CY, KS, SR, RM, and FF wrote the manuscript.

The authors declare no competing financial interests.

Conflict of Interest: The authors state no conflict of interest to declare.

Author Manuscript Author Manuscript Author Manuscript Author Manuscript

Author Manuscript Author Manuscript Author Manuscript Author Manuscript

delta frequency band dominated by infragranular V1 and multiple frequency bands that were most pronounced in supragranular V1. This inter-area coupling was differentially modulated by full-field synthetic and naturalistic visual stimulation. We also found that visual responses in LPl were distinct from the ones in V1 in terms of their reliability. Together, our data support a model of multiple communication channels between the LPl and layers of V1 that are enabled by oscillations in different frequency bands. This demonstration of anatomical and functional connectivity between LPl and V1 in ferrets provides a roadmap for studying the interaction dynamics during behavior and a template for identifying activity dynamics of other thalamic feedback loops.

Keywords

lateral posterior nucleus; pulvinar; multiunit activity; local field potential; oscillations; networks

Introduction

Synchronization of activity across cortical areas represents a fundamental mechanism by which information is routed and processed during cognition and behavior. For example, in attention-demanding tasks, synchronization in specific frequency bands relays relevant information between sensory and higher-order cortical areas (Buschman & Miller, 2007; Gregoriou *et al.*, 2009). Such long-range synchronization may result from direct cortico-cortical interactions or may be orchestrated by subcortical structures that are reciprocally connected with the relevant cortical areas. The pulvinar may represent such a subcortical hub since it organizes cortical network activity in the alpha frequency band (8-12 Hz) in response to attentional demands in non-human primates (Saalmann *et al.*, 2012). Additionally, human neuroimaging data (Kastner *et al.*, 2004; Fischer & Whitney, 2012; Zhang *et al.*, 2013) and lesion reports from human patients (Arend *et al.*, 2008; Snow *et al.*, 2009; Rinne *et al.*, 2013) support a model in which the pulvinar is a key element of the neural substrate of attention and saliency processing. Together these data propose that the pulvinar may act as a hub in large-scale functional networks that process sensory information in primates. Such a hub could gate and route sensory information to meet attentional demands by selectively synchronizing brain areas required for processing of salient sensory input (Grieve *et al.*, 2000).

Reciprocal connectivity has been demonstrated between the pulvinar and primary visual cortex (V1) in the primate (Lund *et al.*, 1975; Benevento & Rezak, 1976; Ogren & Hendrickson, 1977; Jones, 2007; Kaas & Lyon, 2007; Marion *et al.*, 2013). Yet, very little is known about the functional role of this feedback loop. Interestingly, a recent study showed that inactivation of the lateral pulvinar, which projects to V1 in primates, abolished visual responses in superficial layers of V1, suggesting an important role of the pulvinar projections in regulating V1 output (Purushothaman *et al.*, 2012). Yet, the interaction dynamics between the two areas have remained unknown. To fill this gap, we studied the structural and functional connectivity between the LP/pulvinar complex and area 17 (V1) in ferrets. Of note, there remains a considerable neuroanatomical debate about homologies across species. In particular, the structure of the posterior thalamus in carnivores may not

Author Manuscript Author Manuscript Author Manuscript Author Manuscript

map one-to-one onto the primate thalamus (Chalupa, 1977). In ferrets, the LP/pulvinar complex is defined by comparison with the cat (Jones, 2007). Importantly, the lateral aspect of LP (LPl) in the cat is the only subdivision of the LP/pulvinar complex that receives input from and sends projections to areas 17 and 18 (Berson & Graybiel, 1978; Updyke, 1981; Segraves & Rosenquist, 1982; Berson & Graybiel, 1983; Raczkowski & Rosenquist, 1983; Abramson & Chalupa, 1985), comparable with the striate-recipient zone of the primate inferior pulvinar nucleus. Based on these connectivity findings in the cat, LPl in carnivores resembles the primate pulvinar in terms of its connections with the primary visual cortex. Yet, no detailed study of structure, connectivity, or network dynamics of the LPl in ferrets has been reported. We here performed histological staining, anatomical tracing, and electrophysiological studies to delineate the structural and functional connectivity between LPl and V1in the ferret.

Materials and Methods

Surgery

Female ferrets (*Mustela putorius furo*, 16-20 weeks old, 750-1000g) were used for tracer studies (n = 3) and electrophysiological recordings in a single terminal procedure (n = 8). Surgical methods have been previously described in detail elsewhere (Sellers *et al.*, 2013). Briefly, anesthesia was induced with an intramuscular injection of ketamine (30 mg/kg) and xylazine (1-2 mg/kg). Animals were then intubated and anesthesia was maintained with isoflurane administered through mechanical ventilation (0.5% to 1.25% isoflurane, 10-11cc, 50bpm, 100% medical grade oxygen). Xylazine (1.5mg/kg/hr) with 5% dextrose lactated ringer's (4.25mL/hr) was continuously administered intravenously through the cephalic vein. For the survival tracer injection surgeries, no xylazine but a higher isoflurane concentration (1.5 – 2.5%) was used. General anesthesia was maintained throughout surgery and the duration of recordings, as assessed by complete absence of withdrawal response to toe pinch. Physiological signals were continuously monitored (electrocardiogram, partial oxygen saturation, end-tidal CO2, and rectal body temperature). End-tidal CO2 was between 30 and 50 mmHg (Kohn, 1997) for all animals, and the temperature was maintained between 38.0-39.0°C with a water heating blanket. The eyes of the animal were protected during surgery by application of paralube.

Anatomical Tracing

Three female ferrets were used for tracing studies. To determine the projections from V1 to LPl, anterograde tracer was injected in V1. One animal was microinjected with 0.6 μl of AAV5-CaMKII-ArchT-GFP (7.5×10^{12} vg/ml) in two sites of V1 (8.5 mm and 9 mm lateral from the midline and 3 mm anterior from lambda). To explore the layer-specific connections between V1 and LPl, two different strategies were used. In one animal, AAV5-CaMKII-ArchT-mCherry (1×10^{12} vg/ml) was microinjected (0.3 μl) into LPl (13 mm anterior from lambda and 3.8 mm lateral from the midline) for anterograde labeling of projections in V1. Another animal was injected with 0.4 μl of Alexa 488–conjugated cholera toxin subunit B (2.5μg/μl CTB-488, Invitrogen) into LPl for retrograde labeling of projecting cells in V1. All the injections were conducted using a 1 μL Hamilton syringe with an infusion rate of 0.1μl/min. All viral constructs were packaged and titered by the UNC Vector Core Facility.

Author Manuscript Author Manuscript Author Manuscript Author Manuscript

Adequate pain relief and post-surgery monitoring was provided as described previously (Sellers *et al.*, 2013). Animals were euthanized for histology 12 days after injection for CTB tracing and nine (ArchT-GFP) and eleven (ArchT-mCherry) weeks after the procedure for viral injections. All procedures were approved by the UNC – Chapel Hill IACUC and exceed the guidelines set forth by the NIH and USDA.

Histology

Animals were humanely killed with an overdose of sodium pentobarbital and transcardially perfused with 0.1M phosphate buffered saline (PBS) followed by 4% paraformaldehyde in 0.1M PBS for subsequent histological verification of recording locations and histochemical characterization. Following perfusion, the brains were post-fixed for at least 2 days in 4% paraformaldehyde and then transferred to 30% sucrose. The brains of the eight animals used for electrophysiological recordings were cut in 60 μm sections using a vibratome (Vibratome series 3000 plus) or cryostat (VT-1200, Leica Microsystems) and processed for cytochrome oxidase (CO) staining. The staining protocol for CO combined previously published procedures (Wong-Riley, 1979; Wiser & Callaway, 1996). Brain shrinkage was estimated at ∼15% based on the distance measured on sections and the distance between lesions used during the experiment. Recording sites were reconstructed based on known distances from lesion locations. For the histological analysis of the LP/pulvinar complex, 2 ferret brains with six to eight alternating stains of neighboring 50 μm thick cryostat sections were analyzed. Stains of these series were performed according to the following standard protocols: cell stain (Nissl), fiber stain (myelin silver impregnation, (Gallyas, 1979), cytochrome oxidase stain (Wong-Riley, 1979), parvalbumin (anti-parvalbumin, rabbit, 1:2500, Swant PV28), vesicular glutamate transporter 2 (VGluT2; anti-VGlut 2, guinea pig, 1:2000, Millipore AB2251) and acetylcholinesterase (AChE) (Geneser-Jensen & Blackstad, 1971). Imaging was conducted with a Nikon Eclipse 80i widefield microscope. For the tracer injection experiments, the brains were sliced into 50 μm coronal sections and counterstained with DAPI cell labeling. Confocal images of the mounted brain sections were acquired using a laser scanning confocal microscope (LSM 780; Carl Zeiss) equipped with a 10× objective (EC Plan-Neofluar, NA=0.30; Carl Zeiss), a 20× objective (Plan-Apochromat, NA=0.8; Carl Zeiss) and a 40× objective (Plan-Apochromat, NA=1.4; Carl Zeiss). To determine the injection sites, sections were imaged at 10×. The expression at the injection sites was documented at 20×. To examine the labeled cell bodies or fibers in the projection sites, the images of the sections were captured at 40×.

Magnetic Resonance Imaging (MRI)

To facilitate localization and provide a starting point for bridging histology findings with a future MR atlas of the ferret, MRI was performed of a single ferret brain (Figure S1) using a 9.4 Tesla Bruker BioSpec system with a BGA-9S gradient insert and a 35 mm quadrature volume coil used as a transceiver (Bruker Corp., Billerica, MA). After perfusion with a solution of 10% formalin and Magnevist (Bayer Schering Pharma, Montville, NJ) (20:1 ratio), the brain was placed in an aprotic solvent – perfluoropolyether (Fomblin Y04, Kurt J. Lesker Company, Clairton, PA), and scanned with a magnetic resonance microscopy protocol using high-resolution T2-weighted RARE sequence with spectral width=60 kHz,

Author Manuscript Author Manuscript Author Manuscript Author Manuscript

TR/TE=2500/45 msec, FOV=2.8×1.92 cm, slice thickness=0.75 mm, matrix=560×384, RARE factor=8, and averages=100, resulting in spatial resolution of 50×50×750 μm.

Multi-Site Electrophysiology and Visual Stimulation

Surgery provided access to V1 and LPl for electrophysiological recordings. Following an initial midline incision of the scalp, soft tissue was retracted and a craniotomy was drilled over left V1 (3 mm anterior from lambda and 9 mm lateral from the midline) and over left LPl (13 mm anterior from lambda and 3.8 mm lateral from the midline). Furosemide was administered to reduce the likelihood for swelling (1 mg/kg, intramuscular injection). The dura was removed at each craniotomy location and the brain was covered with warm, 4% agar in physiological saline. A stainless steel head post was implanted using bone screws anterior to the LPl craniotomy.

Following the surgical procedure, the animal was positioned in a head-frame for simultaneous electrophysiological recordings in V1 and LPl to record local field potential (LFP) and multiunit activity (MUA) during spontaneous and visually-evoked activity. In V1, activity in all cortical layers was simultaneously recorded with acutely-inserted linear silicon probes (32 channels, 50μm contact site spacing along the z-axis, Neuronexus, Ann Arbor, MI); neural activity in the LPl was recorded using acutely-inserted single metal electrodes (tungsten microelectrode, 250μm shank diameter, 500 kOhms impedance, FHC Inc., Bowdoin, ME). The reference for the V1 electrode was located on the same shank (0.5 mm above the most superficial recording site), and was placed in agar in saline above the surface of cortex. A silver chloride wire positioned between skull and soft tissue and held in place with 4% agar in saline was the reference for the LPl electrode. Each electrode was slowly advanced using a micromanipulator (Narishige, Tokyo, Japan). Separate recording depths for each penetration in LPl were spaced 300-400 μm apart. Probes in V1 were positioned such that superficial electrodes exhibited low amplitude LFP signals and deep electrodes exhibited high amplitude LFP signals; the electrode for the LPl was advanced to approximately 6.5 mm ventral from the surface of cortex after dura was removed. At the conclusion of each penetration, one or two electrolytic lesions (400μm apart in the z-plane) were induced by passing currents (5 μA, 10s, unipolar) through the tips of the metal recording electrodes in LPl.

Unfiltered signals from V1 were amplified with MPA8I head-stages with gain 10 (Multichannel Systems, Reutlingen, Germany) and then amplified with gain 500 (Model 3500, A-M Systems, Carlsborg, WA). Unfiltered signals from the LPl were amplified with gain 1000 (Model 1800, A-M Systems, Carlsborg, WA). All signals were digitized at 20 kHz (Power 1401, Cambridge Electronic Design, Cambridge, UK) and digitally stored using Spike2 software (Cambridge Electronic Design). Upon placement of the recording electrodes, the animal was presented with visual stimulation presented on a 52 × 29cm monitor with a refresh rate of 120Hz (1,920 × 1,080 pixels, GD235HZ, Acer Inc, New Taipei City, Taiwan) at 40 cm distance from the animal, filling 60 degrees of the visual field horizontally (azimuth) and 40 degrees of the visual field vertically (elevation). Visual stimulation was controlled by the Psychophysics toolbox (Brainard, 1997) and a GeForce580 GPU (NVIDIA, Santa Clara, CA). Full-field black and white (randomized)

Author Manuscript Author Manuscript Author Manuscript Author Manuscript

flashes for 33msec, with 967msec interval (300 trials each), were presented during electrophysiological recordings in order to assess visually-evoked potentials. Current source density (CSD) was calculated from responses to the white flashes. A set of different artificial and naturalistic stimuli was presented to the animal to measure network dynamics of sensory processing; each trial consisted of ten seconds of visual stimulation bracketed by ten seconds of gray screen (at 50% contrast). Each stimulus was presented ten times in randomized order. The stimuli included 10 checkerboard frozen noise stimuli presented for 1 second each ("1Hz noise", NOI) and a naturalistic stimulus from a nature video clip of foxes (FOX, Planet Earth, BBC, London, UK). For all stimuli, the timing of individual frames was confirmed by a photodiode covering a small, fully covered, flashing square in the corner of the monitor. In addition, electrophysiological signals were recorded from V1 and the LPl in absence of visual stimulation (typical duration: 10 minutes), when the animal was in the complete dark (spontaneous activity). The eyes of the animal were open during all recordings and moistened with physiological saline prior to the start of each recording.

Electrophysiology Data Analysis

Of the 47 thalamic recording sites, two recording locations could not be accurately localized, nine did not respond to our visual stimulation paradigm, and eight were in the LGN (Figure 5, Figure S2). These 19 sites were excluded from analysis, resulting in a dataset of LFP and MUA from 28 sites in LPl to be analyzed. Neurophysiological data were analyzed with custom-written MATLAB (Mathworks, Natick, MA) scripts. LFP data were extracted by low-pass filtering of the raw broadband signal with a cut-off frequency of 300 Hz. MUA was extracted by applying a threshold of minus-four-times of the standard-deviation to the highpass-filtered neurophysiological data (filter cut-off: 300 Hz, 4^{th} order Butterworth). Visual responses were first determined from full-field black ("off") or white ("on") stimuli presented for 33 msec. Peri-stimulus time histograms (PSTHs) were determined by computing the average spiking response across trials with a bin width of 5 msec. Peak amplitudes were determined as peak MU firing rate in the first 100ms after stimulus onset minus 99% of mean baseline firing rate (500ms) before stimulus onset, averaged across trials. This threshold was chosen to avoid contamination of the response by outlier values in the baseline activity period. Time of the first spike was computed as average time elapsed between stimulus onset and first spike across all trials. Half-peak latency was computed as time elapsed between the stimulus onset and the time point when the response reached 50% of its peak. Spike-count variance was calculated as the variance of the number of spikes occurring between 10 and 150 msec after stimulus onset. Spike-count mean was determined from the same window. Temporal jitter was determined by calculating the standard deviation of the time of the first spike after stimulus onset. Supragranular (Layers L1-L2/3), granular (L4), and infragranular (L5-L6) electrode sites were identified by determining the current-source density (CSD) from the full-field, white stimuli (Rappelsberger *et al.*, 1981; Pettersen *et al.*, 2008). The superficial aspect of the granular layer corresponded to the top of the initial sink elicited by visual stimulation. CSD profiles were spatially smoothed using a Hanning window (Ulbert *et al.*, 2001). Reponses to 10 sec visual stimuli were determined by computing channel-averaged, trial-averaged PSTHs. Firing-rate responses are computed as the ratio of MU firing rate during the stimulus to the MU firing rate in the 10 sec window ("rest") preceding the stimulus.

Author Manuscript Author Manuscript Author Manuscript Author Manuscript

Spectral analysis was performed by convolving the LFP signals with a family of Morlet wavelets (0.5 to 40Hz, step-width of 0.5Hz) and subsequently averaging over time. Spectra are presented on a logarithmic scale. Relative strength of the individual classical EEG frequency bands (delta: 0.5-4Hz; theta: 4-8 Hz; alpha: 8-12 Hz; beta: 12-30 Hz, gamma: 30-40 Hz) was computed by normalizing the mean power in each frequency band with the total power between 0.5-40 Hz (Sellers *et al.*, 2013). Power correlations (Wang *et al.*, 2012) were determined by computing the correlation coefficient between the power in individual 5 sec segments of continuous recordings with averages across channels based on the CSD analysis to split the V1 data into supragranular, granular, and infragranular layers. Magnitude square coherence was determined on the same 5 sec windows and averaged across windows for the spontaneous activity recorded in the dark. Coherence before (REST) and during visual stimulation (NOI and FOX) were calculated from the 10 sec LFP windows before and during visual stimulation. Averages for cortical layers were calculated across channels as for the other analyses. Baseline correction of coherence was conducted by subtracting the coherence of the matched, trial-shuffled data set. Phase preference of MUA was determined by extracting the instantaneous phase of the band pass filtered LFP using the Hilbert transformation (individually for each frequency band) and building the phase histograms for all detected MU spikes in the other brain area. Phase-preference was computed as Kullback-Leibler distance to a matched uniform distribution (Fröhlich & McCormick, 2010). These metrics were determined across all recording sessions to build accurate histograms; error bars are shown as bootstrapped 95% confidence intervals. Phase-preference before and during visual stimulation were calculated from 10 sec windows. If not noted otherwise, results are presented as averages across electrode sites corresponding to supragranular, granular, or infragranular layers in V1 and statistics are performed on the group of trial-averaged individual recordings (electrode locations). Except if when noted otherwise, all statistical tests were performed by using factorial ANOVA (anovan function in Matlab) with post-hoc paired testing if the corresponding main effect or the interaction was significant at $p<0.05$. To control for multiple comparisons, pairwise post-hoc tests were performed with the Tukey's honestly significant different (HSD) test with a $p<0.05$ significance cut-off.

Results

In order to delineate the LP/pulvinar complex in ferrets, we performed a histological characterization of the area with classical histochemical and immuno-histochemical stains. We found that the LP/pulvinar complex in the ferret roughly compares to that of the cat (Fig. 1, representative examples of relevant stains). It is located within the dorsal thalamus medial to the lateral geniculate nucleus (LGN), dorsal to medial geniculate nucleus (MGN) and extends in rostrocaudal dimensions about 4mm from the rostral beginning of the ventrobasal complex to the caudal end of LGN. A large lateral-posterior nucleus (LP) dominates the complex. Judging from distinct differences in chemo- and cytoarchitecture, the LP of the ferret has several subdivisions. Comparable to the cat (Jones, 2007), the most posterior part constitutes the lateral LP (LPl) is easy to delineate as it stains intensely for cytochrome oxidase but weakly for AChE. In the cat, LP has three subdivisions, each with a specific connectivity pattern. LPl is the only subdivision of the LP/pulvinar complex that receives

Author Manuscript Author Manuscript Author Manuscript Author Manuscript

projections from the primary visual cortex (V1, area 17) and area 18 (Berson & Graybiel, 1978; Updyke, 1981; Segraves & Rosenquist, 1982; Berson & Graybiel, 1983; Raczkowski & Rosenquist, 1983). The connectivity of LPl with the primary visual cortex (area 17) and area 18 is reciprocal in the cat. We therefore focused on this subdivision of LP/pulvinar for our study of interaction dynamics between LP/pulvinar and V1 in the ferret.

We then asked if LPl of the ferret exhibits similar anatomical connections between LPl and area 17 (V1) by anatomic tracing. To establish that V1 projects to LPl, we injected AAV5-CaMKII-ArchT-GFP into V1 (Fig. 2A) at the posterior pole of the hemisphere. This location is the same as our electrophysiological recording sites (see Fig.5C). We found densely labelled terminals in a patch of LPl (Fig. 2B and enlargement in 2C) and also a band of expression in LGN. The connectivity pattern is in accord with findings in the cat (Abramson & Chalupa, 1985) and confirms our delineation of LPl.

To further investigate the layer-specific connections between these two areas, we examined projections from V1 to LPl by injecting retrograde tracer CTB488 into LPl (Fig. 3A and B). We found retrograde labeled pyramidal cells in the infragranular layers V/VI of V1 (Fig. 3C-E). To determine the presence of layer specific projections from LPl to V1, we injected anterograde viral tracer AAV5-CaMKII-ArchT-mCherry into LPl (Fig.4A and 4B) and examined the projections in V1 (Fig. 4C and 4D). We found that mCherry-labelled projections densely terminated in layer I of V1, with some termination in III/upper layer IV, but almost none in the infragranular layers. This projection pattern of LPl to area 17 and 18 was described for the cat by several authors (reviewed in Jones, 2007) and further confirms our delineation of LPl. To locate the LP/pulvinar complex of the ferret in the brain, we also performed a structural MRI scan (Fig. S1) as no stereotaxic ferret brain atlas is currently available.

Full-Field Visual Responses

We simultaneously recorded LFP and MUA from the LPl and V1 in absence of visual input (spontaneous activity in the dark) and during presentation of visual stimuli in the anesthetized ferret (Fig. 5A). We used a single metal electrode to record from LPl and a multichannel silicon probe with 32 vertically aligned channels to simultaneously record from all cortical layers in V1. The exact locations of the recording sites were confirmed by electric lesions and subsequent histology (Figs. 5B, 5C, and S2). The eyes of the animals were open during all recordings.

To characterize visual responses, we used full-field white (“on”) and black (“off”) flashes (in randomized order). In order to assess the depth of the multichannel silicon probe in V1 we used current source density (CSD) analysis to locate the current sinks and sources generated by visual response to full-field white flashes across the depth of the cortex (Fig. 5D). The upper end of the superficial current sink was considered as the point of alignment (superficial granular layer) and used for averaging data across recordings.

Twenty eight LPl recording locations (n= 8 animals, examples in Fig.5B and Fig. S2, Table S1) exhibited responses to visual stimulation. MUA increased in response to the onset of the full-field white and black visual stimuli (Fig. 6A, population PSTHs). To quantify and

Author Manuscript Author Manuscript Author Manuscript Author Manuscript

compare the neuronal responses in LPl and V1 across layers (supragranular: L1-L2/3; granular: L4; infragranular: L5-L6), we first determined the peak amplitude of the MUA during “on” and “off” flashes (Fig. 6B, top). In the LPl, MUA exhibited similar peak responses to both flashes ($p>0.05$, rank-sum test). Differently, a two-way ANOVA showed a significant main effect of stimulus type (“on” vs “off”, $F_{1,727} = 244.65$, $p < 0.001$), a significant main effect of recording site (three V1 layers, $F_{2,727}= 13.8$, $p < 0.001$), and no significant interaction between stimulus type and recoding site ($F_{2,727} = 2.44$, $p >0.05$) among the three V1 layers. According to post-hoc comparisons, for ‘’on” flashes, the peak amplitude of MUA in supragranular layers was significantly lower than in granular and infragranular layers ($p<0.05$). For “off” flashes, peak amplitude of MUA was not significantly different among V1 layers (supragranular, mean = 60.4Hz, granular, mean = 90.5Hz, infragranular, mean = 74.7Hz, $p > 0.05$). We examined timing of the first spike (measured from stimulus onset to first spike) during “on” and “off” flashes (Fig 6B, bottom). A two-way ANOVA with stimulus type (“on” or “off”) and recording site (LP/pulvinar, V1 cortical layers) as factors revealed a significant main effect of recording site ($F_{3,1124} = 44.85$, $p < 0.001$), main effect of stimulus type ($F_{1,1124} = 128.49$, $p < 0.001$), and a significant interaction between these factors ($F_{3, 1124} = 3.31$, $p = 0.020$). Post-hoc comparison showed that the occurrence of the first spike in LPl MUA (“on”, mean = 54 msec) was significantly later than those of V1 granular and infragranular MUA ($p<0.05$, granular, “on”, mean = 30 msec; infragranular, “on”, mean= 31 msec) during “on” flashes, but not significantly different from those of supragranular MUA (supragranular, “on”, mean = 47 msec). Whereas during “off” flashes, time of the first spike of LPl MUA (“off”, mean = 65 msec) was only statistically different from those of V1 granular neurons (“off”, mean = 49 msec, $p<0.05$), but not those of supragranular and infragranular neurons (supragranular, “off”, mean= 68 msec; infragranular, “off”, mean= 60 msec). To confirm these findings, we also examined response latency measured from stimulus onset to half of response peak during “on” and “off” flashes. A two-way ANOVA with stimulus type and recording site as factors revealed a significant main effect of recording site ($F_{3,774} = 23.18$, $p < 0.001$), no main effect of stimulus type ($F_{1,776} = 0.44$, $p = 0.51$), and a significant interaction between these factors ($F_{3, 774} = 4.08$, $p = 0.007$). Post-hoc comparison showed that latencies of LPl MUA (“on”, mean = 60 msec; “off” mean = 51 msec) were significantly longer than those of V1 neurons ($p<0.05$, supragranular, “on”, mean = 33 msec; “off”, mean = 36 msec; granular, “on”, mean = 31 msec; “off”, mean = 38 msec; infragranular, “on”, mean = 31 msec; “off”, mean = 39 msec). This latter metric of onset delay measures a slightly different feature of the response and may be more robust than the time of the first spike. Nevertheless, the overall picture was the same that V1 has shorter response latencies than LPl (with the potential exception of supragranular layers).

We next sought to further delineate the differences in visual processing between LPl and the different layers in V1; we assessed variability of overall spike count and of spike-timing. We measured spike-count variability to assess the trial-to-trial spike reliability by computing the mean and variance of the spike-count across 300 trials from each stimulus for each MUA recording for both “on” and “off” conditions (Fig. 6C). The variance scaled with the mean spike-count in V1 during both conditions (supragranular, “on”, slope = 0.80, confidence interval, CI = [0.78 0.83]; “off”, slope = 1.03, C I= [0.96 1.10]; granular, “on”, slope = 0.67,

Author Manuscript Author Manuscript Author Manuscript Author Manuscript

CI = [0.62 0.72; “off”, slope=1.34, CI=[1.16 1.53]; infragranular, “on”, slope=0.74, CI=[0.61 0.87]; “off”, slope=1.31, CI=[1.14 1.48]). In contrast, the response in LPl exhibited higher variance as a function of the mean spike-count (“on”, slope = 2.70, CI= [2.02 3.39]; “off”, slope = 3.56, CI = [2.84 4.27]). Thus, LPl responses to full-field visual stimuli were less reliable than V1 responses. We then examined the ability of LPl and V1 MUA to respond with high temporal precision from trial to trial by computing the jitter in the timing of the first spike after stimulus onset for both “on” and “off” stimuli (Fig. 6D). A two-way ANOVA showed a significant effect of stimulus type ($F_{1, 1122} = 58.18$, $p < 0.001$) and significant effect of recording site ($F_{3, 1122} = 57.12$, $p < 0.001$). There was no significant interaction between these factors ($F_{3, 1122} = 1.20$, $p = 0.28$). Thus, in comparison to neurons in V1, LPl MUA exhibited a larger temporal variability in both conditions (“on” jitter: mean = 35 msec, “off” jitter: mean = 48 msec, $p < 0.05$). Meanwhile, supragranular neurons also showed significantly higher temporal jitter than granular and infragranular neurons ($p < 0.05$). Together, these data demonstrate that visual responses are overall less reliable in LPl than in V1, in agreement with the putative role of LP/pulvinar as a higher-order thalamic structure. However, the similarity of LPl and supragranular layers in V1 in terms of more pronounce jitter (in contrast to the more reliable granular and infragranular layers), may suggest closer interaction of LPl with supragranular layers of V1.

Spontaneous Oscillation Dynamics of the LFP

We next analyzed the mesoscale (LFP) interactions between LPl and V1 to elucidate the functional connectivity. We examined the LFP spectral composition of the two areas individually and assessed the correlation between them. In absence of visual input (spontaneous activity), power spectra of both LPl and V1 (all layers) showed pronounced power at low frequencies (< 4 Hz, delta band), likely reflecting the fact that the recordings were performed under anesthesia (Fig. 7A). In addition, the LFP recorded in LPl displayed a clear spectral peak in the gamma frequency band (∼30 Hz). V1 LFP (all three layers) did not exhibit a gamma peak but instead a modest spectral peak (∼25 Hz) in the beta frequency band (12-30 Hz). To further probe these similarities and differences in frequency structure, we analyzed the relative contributions of the different frequency bands to the overall power of the LFP signal (Fig. 7B) by computing the power in each frequency band as a percentage of total power. This normalization avoids potential confounds introduced by amplitude differences caused by the recording systems used in the two areas. Two-way ANOVA showed significant main effects of frequency band (delta, theta, alpha, beta, and gamma, $F_{4, 500} = 1892.42$, $p < 0.001$) and no main effect of recording site ($F_{3, 500} = 0$, $p = 1.00$) for LFP spectral power. There was significant interaction between these factors ($F_{12, 500} = 11.89$, $p < 0.001$). Pair-wise comparisons confirmed the following findings from visual inspection of the spectra: (i) the largest contribution to the overall spectrum in both areas by oscillations in the delta frequency band ($p < 0.05$); (ii) the relative contributions of power in the delta and theta bands were significantly lower in LPl compared with all three cortical layers ($p < 0.05$); and (iii) the relative gamma power in LPl was higher than that in all cortical layers ($p < 0.05$). Distribution of oscillatory power across frequency bands did not differ across V1 layers ($p > 0.05$).

Author Manuscript Author Manuscript Author Manuscript Author Manuscript

Functional Connectivity of LPl and V1 at the LFP Level

To study the functional connectivity between LPl and V1 as a function of oscillatory activity, we applied the MRI resting state analysis strategy of assessing the correlations of spontaneous fluctuations of activity levels measured by oscillation power as a function of frequency band (Wang *et al.*, 2012). Specifically, we investigated LFP power correlations between the LPl and each V1 cortical layer by performing a correlation analysis of LFP spectral power at different frequency band during spontaneous activity (i.e. dark, no visual input) (Fig. 7C and 7D). We divided the continuous recordings into 5 second segments, computed the correlation coefficients between the spectral powers, and averaged across channels corresponding to supragranular, granular, or infragranular layers. We found a significant main effect of frequency band (two-way ANOVA, $F_{4, 376} = 5.21$, $p < 0.001$), in which there were significantly higher correlations in alpha power between the LPl and all three cortical layers compared with delta, theta, beta, and gamma power (Fig. 7D). Although the power values in LPl and supragranular layer displayed higher alpha correlations, only trend-level correlation differences were found between LPl and cortical layers ($F_{2,376} = 2.76$, $p = 0.07$). Also, no significant interaction was found between frequency band and different LPl-cortical pairs ($F_{8, 376} = 0.59$, $p = 0.79$). Thus, such time-averaged assessment of functional interaction by frequency-band suggests the alpha frequency band is the key mediator of functional connectivity in absence of visual input.

Motivated by this frequency-specific functional connectivity established by the correlation of slow fluctuations in alpha band power (at the time-scale of seconds), we next computed magnitude square coherence (“coherence”) to establish frequency-specific correlations between the LPl and V1 LFP at a finer (millisecond) time scale. The coherence values were normalized by subtracting the coherence for a matched, trial-shuffled dataset. Coherence exhibited a pronounced peak in the delta frequency band and two smaller peaks at alpha and gamma frequency bands (Fig. 8A, coherence as a function of depth; 8B, depth-averaged coherence; 8C, coherence by frequency band). Two-way ANOVA identified that coherence was significantly affected by LPl-V1 pairs ($F_{2, 315} = 3.91$, $p = 0.02$). Coherence between LPl and V1 supragranular layer was significantly stronger than coherence between LPl and V1 infragranular layers ($p < 0.05$). The main effect of frequency band was also significant ($F_{4, 315} = 44.04$, $p < 0.001$). We found pronounced coherence in the delta band and moderate coherence in the alpha and theta bands, and weak coherence in the beta and gamma frequency bands. There was no significant interaction between location and frequency band ($F_{8, 315} = 0.23$, $p = 0.99$).

Functional Connectivity by Spike-Phase Coupling

Given the frequency-specific coupling between the LPl and V1 at the spatial scale of LFP signals, we asked if functional connectivity spanning LFP and MUA measurements was also present. Specifically, we asked if spikes in V1 exhibited a preferred LPl LFP phase and vice versa. We found strong and selective phase preference for V1 MUA in the delta band of the LPl LFP (Fig. 9A, top: spike-phase histograms; bottom: KL divergence as measure of non-uniformity of spike-phase distribution; Delta, CI of supra= [0.0023, 0.0025]; CI of granular= [0.0070, 0.0072]; CI of infra= [0.0150, 0.0152]). This coupling in the delta frequency band scaled with cortical depth such that MUA in infragranular layers exhibited the strongest

Author Manuscript Author Manuscript Author Manuscript Author Manuscript

phase preference. Given the anatomical projections from deep cortical layers to LPl (Fig. 3), the scaling of the spike-preference with cortical depth reflects the importance of cortico-thalamic projections in generating slow cortical oscillations. In the case of LPl MUA, we found that all frequency bands of the cortical LFP shaped the spike-timing of LPl MUA (Fig. 9B: LPl MUA as a function of V1 LFP phase). Consistent across frequency bands, such functional connectivity was strongest for supragranular layers (for example, in the delta frequency band: CI of supra= [0.0116, 0.0119]; CI of granular= [0.0081, 0.0083]; CI of infra= [0.0052, 0.0053]), in agreement with the anatomical projections of LPl to superficial cortical layers that we found in our tracing study. These data also agree with the power correlation and the LFP coherence analysis that similarly showed stronger functional connectivity for the superficial layers. To confirm that the LFPs recorded in LPl and V1 layers were not signals from neighboring structures, we also computed spike-phase locking within each area (Fig. S3A). These results excluded the possibility that LFP recoded in LPl is limited to volume transmission from LGN.

Network Dynamics in Response to Synthetic and Naturalistic Visual Input

Little is known about how LPl responds to dynamic, full-field visual stimulation. To fill this gap, we presented two types of 10 sec visual stimuli (Fig. 10A): 1Hz checkerboard frozen noise (NOI, “synthetic/artificial”) and a nature movie clip with foxes (FOX, “naturalistic”). Synthetic visual stimuli represent a key tool for the study of visual responses, yet “naturalistic” visual input may engage different processing mechanisms (Simoncelli & Olshausen, 2001; Felsen & Dan, 2005). We compared MUA responses between the two stimuli in LPl and V1 layers (Fig. 10B and 10C). MUA in LPl caused similar responses to NOI and FOX ($p>0.05$, t-test). Using a two- way ANOVA with stimulus type and recording site as factors, we found that normalized MUA responses in V1 layers were significantly affected by stimulus type (main effect of stimulus, $F_{1, 102} =10.1$, $p <0.005$, no effect of recording site, $F_{2,102} = 0$, $p >0.05$, no significant interaction, $F_{2,102} = 0$, $p >0.05$), in which V1 MUA was higher during naturalistic stimulation than during artificial stimulation (Fig. 10D).

To probe whether synthetic and naturalistic visual stimuli differentially modulated functional interactions between LPl and V1, we next examined the modulation of spike-phase locking between LPl and V1 at the level of LFP and MUA (same analysis strategy as in Fig. 9). First, we quantified the LFP spectral characteristics of LPl and V1 before and during the visual stimulation (Fig. 11). Similar to the spectral structure during spontaneous activity (Fig. 7), power spectra before (REST) and during visual stimulation (NOI and FOX) showed pronounced power in the delta band (< 4 Hz) in both LPl and V1 (all layers), and a clear spectral peak in the gamma band in LPl (∼30 Hz).

Next, we probed for differential effects of synthetic and naturalistic visual stimulation on the spike-phase coupling between LPl and V1. We first examined V1spike and LPl LFP phase preferences during the NOI and FOX visual stimulation in comparison to the phase preference during REST (Fig. 12). We found that the layer-specific phase preference for cortical MUA in the delta band of the LPl LFP was clearly modified during both NOI and FOX visual stimulation (Fig. 12A, KL divergence as measure of non-uniformity of spike

Author Manuscript Author Manuscript Author Manuscript Author Manuscript

phase during the REST; delta, CI of supra= [0.0018, 0.0021]; CI of granular= [0.0054, 0.0060]; CI of infra= [0.0151, 0.0158]). During the NOI stimulation, phase preferences were reduced in infragranular layer, but increased in supragranular layer in the delta band (delta, CI of supra= [0.0090, 0.0095]; CI of granular= [0.0052, 0.0056]; CI of infra= [0.0099, 0.0103]). Meanwhile, phase preference in the other frequency bands was increased with no distinct differences between layers. In contrast, during naturalistic visual stimulation, the layer-specific phase preference was only reduced in the delta band and we observed no clear changes in the other frequency bands during the FOX stimulation (delta, CI of supra= [0.0016, 0.0019]; CI of granular= [0.0025, 0.0027]; CI of infra= [0.0022, 0.0023]).

In the case of LPl MUA, we found that all frequency bands of the cortical LFP were coupled to the spike-timing of LPl MUAs during two types of visual stimuli and the strongest connectivity was still found in supragranular layers across frequency bands (Fig. 12B). Interestingly, the NOI stimulus and FOX stimulus produced opposite influence on the phase preference, in which NOI increased phase preference and FOX reduced phase preference across all the frequency. Phase preference during the REST condition was comparable to the results shown during the spontaneous activity (Fig. 9). To examine the modulation of local spike- phase synchronization, we also computed spike-phase distributions for all frequency bands within each area during REST, NOI and FOX (Fig. S3B). Similar to cross-area phase preference, NOI stimulus strengthened phase preference, while FOX stimulus weakened the phase preference. The phase preferences within LPl were not affected by visual stimuli. These data suggest that different visual stimuli not only caused different levels of MUA and LFP fluctuation but also imposed different functional connectivity between LPl and V1.

Discussion

We characterized the LPl of the LP/pulvinar complex and its layer-specific interaction dynamics with area 17 (V1) in ferrets, a model system with a relatively well-developed visual system including higher-order cortical visual areas (Law *et al.*, 1988; Manger *et al.*, 2002a; Manger *et al.*, 2002b; Manger *et al.*, 2010; Patzke *et al.*, 2014). We found (1) a histochemical substructure of the ferret LP/pulvinar complex (LPl) that is reciprocally connected with V1 in the ferret, (2) the LPl robustly responded to full-field synthetic and naturalistic visual input, (3) frequency- and layer-specific functional connections between the LPl and V1, and (4) the functional interactions between LPl and V1 were differentially modulated by different types of visual stimulation.

The visual thalamus consists of two main nuclei that project to cortex. LGN is a first-order thalamic nucleus that has been extensively studied in terms of its anatomical connectivity patterns, response properties and strength of oscillatory activity (Jones, 2007; Saalmann & Kastner, 2011). However, to our knowledge, the LP/pulvinar has not been previously studied in ferrets and therefore the comparison with other species provides important insights. However, there are discrepancies in nomenclature between the primate and the carnivore literature. The LP/pulvinar complex shows large variations between mammalian species as the pulvinar nucleus largely expands in size and differentiation with progressive evolutionary development of the neocortex, whereas LP decreases. The main subdivisions in the primate pulvinar are the lateral, medial, and inferior pulvinar. In contrast, in the cat,

Author Manuscript Author Manuscript Author Manuscript Author Manuscript

seemingly similar structures have been referred to as subdivisions of the lateral-posterior nucleus (LP), with a fourth, poorly characterized nucleus referred to as pulvinar (Jones, 2007). The nuclei of pulvinar and LP are neighboring structures, and to some extent resemble each other in histological appearance and connectivity, however, equivalent nuclei may not always have been recognized as such in different species (for review see Jones, 2007, chapter 10) (Jones, 2007). Inhomogeneous nomenclature is used for the subdivisions of the LP/pulvinar complex between species and inconsistent naming is used by different authors for a given species. The LP/pulvinar complex of the ferret has been drawn in figures of several earlier studies that focused on other brain areas (Herbert, 1963; Pallas *et al.*, 1990; Angelucci *et al.*, 1997; Manger *et al.*, 2002b; Highley *et al.*, 2003; Allman *et al.*, 2009; Manger *et al.*, 2010; Vazquez-Garcia *et al.*, 2014). However, criteria used for subdivision schemes are either not explicitly provided or unclear. In contrast, Jones (Jones, 2007) describes the LP/pulvinar complex in the ferret thalamus in comparison to that of the cat based on sections stained for AChE and calcium-binding proteins. In our study, we followed Jones in terms of localization and terminology. Based on classical, histochemical, and immuno-histochemical stains we delineated LPl of the ferret as an intensely cytochrome oxidase- and faintly AChE-stained subdivision of the caudo-lateral LP/pulvinar corresponding to that in the cat, a related carnivore. Besides structural features, each subdivision of the LP/pulvinar complex was also defined by a characteristic connectivity pattern. We here performed a tracing study and showed a correspondence of LPl connectivity pattern in the ferret with the one of the cat. Specifically, we showed that LPl projects to area 17 and vice versa by using anterograde virus and retrograde tracer injections. Concerning the layer specificity of the projections from V1 to LPl, our results show involvement of layer V and VI cells, which differs from what is described in the cat (Abramson & Chalupa, 1985). These authors describe the cells projecting to LPl from area 17 and 18 as layer V pyramidal cells. Whether this mismatch is a species difference or due to a different assessment of the location of the visual areas between authors cannot be determined from our data.

Our electrophysiological characterization of the LPl revealed visually responsive MUA with late onsets, and higher variability both in terms of spike-timing and overall spike count (Fig. 5). Motivated by the demonstration of behaviorally important functional connectivity between the pulvinar area and visual cortices during cognitive tasks (Saalmann *et al.*, 2012), we here asked if functional connectivity between LPl and V1 exists in absence of behavior, during anesthesia characterized by complete loss of consciousness, and how it is altered by full-field visual input. To our knowledge, our study is the first demonstration of layer-specific functional connectivity between the LPl and V1. Importantly, our findings overall agree with what we predicted from our tracer injections and the canonical structural connectivity between cortical circuits and higher-order thalamic structures (Sherman, 2007). In essence, we found functional connectivity between the LPl and both deep (infragranular) and superficial (supragranular) layers of V1. Three frequency bands stood out in our data: delta (< 4 Hz), alpha (8-12 Hz), and gamma (> 30 Hz). The prominence of activity in the delta frequency band is likely the result of anesthesia (Sellers *et al.*, 2015) although similar low-frequency orchestration of cortical network activity may occur also in the awake, resting animal (Poulet & Petersen, 2008; Harris & Thiele, 2011). Second, functional

Author Manuscript Author Manuscript Author Manuscript Author Manuscript

interactions in the alpha frequency band are in agreement with the canonical view that oscillations in the alpha frequency band emerge from cortico-thalamic dynamics (da Silva *et al.*, 1973). Such coherence in the alpha frequency band is consistent with the proposed role of the pulvinar in regulating cortical information flow during attentional states in the awake behaving primate (Saalmann *et al.*, 2012) and with the power fluctuations described for pulvinar and higher-order cortical areas in the resting state (Wang *et al.*, 2012). Third, we found interactions in the gamma frequency band which may reflect wider organization of network activity across areas by fast oscillations.

To further understand the functional interactions during visual processing, we presented synthetic and naturalistic visual stimuli while recording the neural activity from LPl and V1. Synthetic visual stimuli have a long history in vision neuroscience since they elicit robust neuronal responses. Yet, visual circuits in the brain are assumed to be optimized for stimuli similar to the ones used during naturalistic visual stimulation (Simoncelli & Olshausen, 2001; Felsen & Dan, 2005). We found a strong enhancement of low frequency activity in V1 that reflected the temporal structure of the NOI stimulus. Interestingly, these differences were not observed in LPl. Furthermore, we found that spike-phase synchrony between V1 and LPl were increased during NOI stimulation (Figure 12), which may imply that the response to the synthetic visual input dominated over endogenous interaction dynamics between V1 and LPl during presentation of synthetic stimuli. Differently, spike-phase coupling between these two areas was reduced during FOX stimulation (Figure 12). This may reflect the fact that naturalist stimuli exhibit more complex spatio-temporal statistics that require more complex neuronal representation. We speculate that decreased macroscopic coupling, which implies higher entropy, facilitates the processing of naturalistic input.

Our recordings were performed under anesthesia. In theory, neural information processing in the LP/pulvinar may be different in the awake animal and thus the electrophysiological data presented here need to be interpreted with caution. Clearly, anesthesia alters micro- and mesoscale network dynamics (Sellers *et al.*, 2013), yet, at least at the level of global, resting state connectivity assayed by functional MRI, anesthesia may not alter overall functional connectivity (Vincent *et al.*, 2007). Performing these experiments under anesthesia enabled us to assay functional connectivity unperturbed by changes in overall brain state. Functional connectivity emerges at the intersection of the anatomical substrate (unaltered by anesthesia) and the overall activity state (altered by anesthesia). Indeed, our connectivity results are consistent with predictions based on the connections we found in our anatomical studies and predictions based on the overall state of a fully anesthetized animal (strong presence of delta oscillations). Nevertheless, further study of functional connectivity in the awake animal represents an important future direction.

The LP/pulvinar is a higher-order thalamic nucleus and exhibits extensive bidirectional anatomical connections with cortex. The functional role of these cortico-thalamo-cortical connections has remained mostly unclear. Two opposing conceptual frameworks of how higher-order thalamic nuclei and cortical areas interact have been proposed. The key dichotomy in these models boils down to the relative importance of cortico-cortical versus cortico-pulvino-cortical connections for driving cortical areas. For example, in the visual

Author Manuscript Author Manuscript Author Manuscript Author Manuscript

system, area V2 receives input from both the pulvinar and from V1, with most of the afferents localizing in input layer 4 of V2 (Purushothaman *et al.*, 2012). A major debate focuses on the relative strength and functional relevance of these two inputs to V2 (Schiller & Malpeli, 1977; Felleman & Van Essen, 1991; Kaas & Lyon, 2007), and more generally spoken, on the question of whether the pulvinar acts as a driver or a modulator of visual areas (Sherman & Guillery, 2002; Theyel *et al.*, 2010; Sherman, 2012). Despite the fact that the defining physiological and molecular marker for drivers and modulators remains to be determined, it appears that pulvinar input to V2 resembles LGN-V1 connectivity based on vesicular glutamate transporter Vglut2 expression and larger synaptic bouton size, suggesting that the pulvinar is a driver of V2 (Marion *et al.*, 2013). In contrast to V2, it is commonly assumed that the LGN drives V1. The input from pulvinar to V1 would therefore be by definition a modulatory input, yet a recent study demonstrated a powerful effect of pharmacologically blocking lateral pulvinar in terms of eliminating orientation tuning and visual responses in superficial V1 in a primate model (Purushothaman *et al.*, 2012).

It is therefore worthwhile to compare our electrophysiological results to the known anatomical connections of V1 with the pulvinar in other species. Specifically, Layer 5B of V1 connects to the pulvinar (Lund *et al.*, 1975; Ogren & Hendrickson, 1977) and projections from the pulvinar to V1 target layers 1 and 2 (Benevento & Rezak, 1976) in the primate. We hypothesized that these anatomical connections constrain the functional connectivity between the pulvinar and V1. Indeed, our findings overall agree with what is predicted from the canonical structural connectivity between cortical circuits and higher-order thalamic structures (Sherman, 2007). In this model, layer 5 of a primary sensory cortex drives higher-order thalamic nuclei such as the pulvinar. In return, the high-order nucleus provides projections back to layer 1 of V1. However, our electrophysiological recordings do not allow resolution of individual supragranular and infragranular layers. In essence, we found functional connectivity between the LPl and both deep (infragranular) and superficial (supragranular) layers of V1. Although our results do not provide a definite answer to the question of whether the LP/pulvinar is a driver or modulator of V1, the presence of layer-specific functional connections between the two brain areas supports the importance of this connection for neural processing, even in absence of visual input.

To our knowledge, the data presented here represents the first description of the functional network interactions between the LP/pulvinar and V1 in any species. Elucidating functional connectivity has evolved into a key approach for understanding both how physiological and pathological states emerge in complex, interconnected networks (Rubinov & Sporns, 2010). Specific interaction dynamics as found here likely represent the fundamental mechanism by which information is selectively routed in brain networks. Our study describes several specific functional connections between the LP/pulvinar and V1. Combining micro- and mesoscopic electrophysiological assays with high temporal precision enabled us to provide this novel map of functional connectivity in this cortico-thalamo-cortical circuit. Interestingly, changes to the morphology and function of the pulvinar have been associated with a number of neurological and psychiatric disorders (Karnath *et al.*, 2002; Highley *et al.*, 2003; Baldauf *et al.*, 2005; Andrews *et al.*, 2006; Rosenberg *et al.*, 2006; Burlina *et al.*, 2008; Kim *et al.*, 2008; Coscia *et al.*, 2009; Cronenwett & Csernansky, 2010; Li *et al.*,

Author Manuscript Author Manuscript Author Manuscript Author Manuscript

2012). It remains to be seen how impairment of cortico-thalamo-cortical loops contributes to these disease processes, possibly as a substrate of thalamo-cortical “dysrhythmias” (Llinas *et al.*, 1999).

Supplementary Material

Refer to Web version on PubMed Central for supplementary material.

Acknowledgments

The authors thank the members of the Frohlich Lab for their support, in particular Stephen Schmidt for his programming expertise, and the laboratory of Dr. Casagrande at Vanderbilt University for assistance with histochemical protocols. The authors appreciate the helpful input on an earlier version of the manuscript by Dr. Ehud Ahissar. The authors gratefully acknowledge the funding sources; the work was in part funded by a donation by Dean and Brenda Proctor and in part by the National Institute of Mental Health of the National Institutes of Health under Award Number R01MH101547. The content is solely the responsibility of the authors and does not necessarily represent the official views of the National Institutes of Health. Imaging was supported by the Confocal and Multiphoton Imaging Core of NINDS Center Grant P30 NS045892.

References

Abramson BP, Chalupa LM. The laminar distribution of cortical connections with the tecto- and cortico-recipient zones in the cat's lateral posterior nucleus. Neuroscience. 1985; 15:81–95. [PubMed: 4010937]

Allman BL, Keniston LP, Meredith MA. Adult deafness induces somatosensory conversion of ferret auditory cortex. Proceedings of the National Academy of Sciences of the United States of America. 2009; 106:5925–5930. [PubMed: 19307553]

Andrews J, Wang L, Csernansky JG, Gado MH, Barch DM. Abnormalities of thalamic activation and cognition in schizophrenia. The American journal of psychiatry. 2006; 163:463–469. [PubMed: 16513868]

Angelucci A, Clasca F, Bricolo E, Cramer KS, Sur M. Experimentally induced retinal projections to the ferret auditory thalamus: development of clustered eye-specific patterns in a novel target. The Journal of neuroscience : the official journal of the Society for Neuroscience. 1997; 17:2040–2055. [PubMed: 9045732]

Arend I, Rafal R, Ward R. Spatial and temporal deficits are regionally dissociable in patients with pulvinar lesions. Brain: a journal of neurology. 2008; 131:2140–2152. [PubMed: 18669494]

Baldauf ZB, Chomsung RD, Carden WB, May PJ, Bickford ME. Ultrastructural analysis of projections to the pulvinar nucleus of the cat. I: Middle suprasylvian gyrus (areas 5 and 7). The Journal of comparative neurology. 2005; 485:87–107. [PubMed: 15776451]

Benevento LA, Rezak M. The cortical projections of the inferior pulvinar and adjacent lateral pulvinar in the rhesus monkey (Macaca mulatta): an autoradiographic study. Brain research. 1976; 108:1–24. [PubMed: 819095]

Berson DM, Graybiel AM. Parallel thalamic zones in the LP-pulvinar complex of the cat identified by their afferent and efferent connections. Brain research. 1978; 147:139–148. [PubMed: 656909]

Berson DM, Graybiel AM. Organization of the striate-recipient zone of the cats lateralis posterior-pulvinar complex and its relations with the geniculostriate system. Neuroscience. 1983; 9:337–372. [PubMed: 6877598]

Brainard DH. The Psychophysics Toolbox. Spatial vision. 1997; 10:433–436. [PubMed: 9176952]

Burlina AP, Manara R, Caillaud C, Laissy JP, Severino M, Klein I, Burlina A, Lidove O. The pulvinar sign: frequency and clinical correlations in Fabry disease. Journal of neurology. 2008; 255:738–744. [PubMed: 18297328]

Buschman TJ, Miller EK. Top-down versus bottom-up control of attention in the prefrontal and posterior parietal cortices. Science. 2007; 315:1860–1862. [PubMed: 17395832]

Author Manuscript Author Manuscript Author Manuscript Author Manuscript

Chalupa LM. A review of cat and monkey studies implicating the pulvinar in visual function. Behavioral biology. 1977; 20:149–167. [PubMed: 409388]

Coscia DM, Narr KL, Robinson DG, Hamilton LS, Sevy S, Burdick KE, Gunduz-Bruce H, McCormack J, Bilder RM, Szeszko PR. Volumetric and shape analysis of the thalamus in first-episode schizophrenia. Human brain mapping. 2009; 30:1236–1245. [PubMed: 18570200]

Cronenwett WJ, Csernansky J. Thalamic pathology in schizophrenia. Current topics in behavioral neurosciences. 2010; 4:509–528. [PubMed: 21312411]

da Silva FH, van Lierop TH, Schrijer CF, van Leeuwen WS. Organization of thalamic and cortical alpha rhythms: spectra and coherences. Electroencephalography and clinical neurophysiology. 1973; 35:627–639. [PubMed: 4128158]

Felleman DJ, Van Essen DC. Distributed hierarchical processing in the primate cerebral cortex. Cerebral cortex. 1991; 1:1–47. [PubMed: 1822724]

Felsen G, Dan Y. A natural approach to studying vision. Nature neuroscience. 2005; 8:1643–1646. [PubMed: 16306891]

Fischer J, Whitney D. Attention gates visual coding in the human pulvinar. Nature communications. 2012; 3:1051.

Fröhlich F, McCormick DA. Endogenous electric fields may guide neocortical network activity. Neuron. 2010; 67:129–143. [PubMed: 20624597]

Gallyas F. Simultaneous determination of the amounts of metallic and “reducible” silver in histologic specimens. Histochemistry. 1979; 64:77–86. [PubMed: 93095]

Geneser-Jensen FA, Blackstad TW. Distribution of acetyl cholinesterase in the hippocampal region of the guinea pig. I. Entorhinal area, parasubiculum, and presubiculum. Zeitschrift fur Zellforschung und mikroskopische Anatomie. 1971; 114:460–481. [PubMed: 5550728]

Gregoriou GG, Gotts SJ, Zhou H, Desimone R. High-frequency, long-range coupling between prefrontal and visual cortex during attention. Science. 2009; 324:1207–1210. [PubMed: 19478185]

Grieve KL, Acuña C, Cudeiro J. The primate pulvinar nuclei: vision and action. Trends in neurosciences. 2000; 23:35–39. [PubMed: 10631787]

Harris KD, Thiele A. Cortical state and attention. Nature reviews Neuroscience. 2011; 12:509–523. [PubMed: 21829219]

Herbert J. Nuclear structure of the thalamus of the ferret. The Journal of comparative neurology. 1963; 120:105–127. [PubMed: 13953890]

Highley JR, Walker MA, Crow TJ, Esiri MM, Harrison PJ. Low medial and lateral right pulvinar volumes in schizophrenia: a postmortem study. The American journal of psychiatry. 2003; 160:1177–1179. [PubMed: 12777280]

Jones, EG. The thalamus. Cambridge University Press; Cambridge; New York: 2007.

Kaas JH, Lyon DC. Pulvinar contributions to the dorsal and ventral streams of visual processing in primates. Brain research reviews. 2007; 55:285–296. [PubMed: 17433837]

Karnath HO, Himmelbach M, Rorden C. The subcortical anatomy of human spatial neglect: putamen, caudate nucleus and pulvinar. Brain : a journal of neurology. 2002; 125:350–360. [PubMed: 11844735]

Kastner S, O'Connor DH, Fukui MM, Fehd HM, Herwig U, Pinsk MA. Functional imaging of the human lateral geniculate nucleus and pulvinar. J Neurophysiol. 2004; 91:438–448. [PubMed: 13679404]

Kim DJ, Kim JJ, Park JY, Lee SY, Kim J, Kim IY, Kim SI, Park HJ. Quantification of thalamocortical tracts in schizophrenia on probabilistic maps. Neuroreport. 2008; 19:399–403. [PubMed: 18287935]

Kohn, DF. Anesthesia and analgesia in laboratory animals. Academic Press; San Diego: 1997.

Law MI, Zahs KR, Stryker MP. Organization of primary visual cortex (area 17) in the ferret. The Journal of comparative neurology. 1988; 278:157–180. [PubMed: 3068264]

Li X, Sroubek A, Kelly MS, Lesser I, Sussman E, He Y, Branch C, Foxe JJ. Atypical pulvinar-cortical pathways during sustained attention performance in children with attention-deficit/hyperactivity disorder. Journal of the American Academy of Child and Adolescent Psychiatry. 2012; 51:1197–1207. e1194. [PubMed: 23101745]

Author Manuscript Author Manuscript Author Manuscript Author Manuscript

Llinas RR, Ribary U, Jeanmonod D, Kronberg E, Mitra PP. Thalamocortical dysrhythmia: A neurological and neuropsychiatric syndrome characterized by magnetoencephalography. Proceedings of the National Academy of Sciences of the United States of America. 1999; 96:15222–15227. [PubMed: 10611366]

Lund JS, Lund RD, Hendrickson AE, Bunt AH, Fuchs AF. The origin of efferent pathways from the primary visual cortex, area 17, of the macaque monkey as shown by retrograde transport of horseradish peroxidase. The Journal of comparative neurology. 1975; 164:287–303. [PubMed: 810501]

Manger PR, Kiper D, Masiello I, Murillo L, Tettoni L, Hunyadi Z, Innocenti GM. The representation of the visual field in three extrastriate areas of the ferret (Mustela putorius) and the relationship of retinotopy and field boundaries to callosal connectivity. Cerebral cortex. 2002a; 12:423–437. [PubMed: 11884357]

Manger PR, Masiello I, Innocenti GM. Areal organization of the posterior parietal cortex of the ferret (Mustela putorius). Cerebral cortex. 2002b; 12:1280–1297. [PubMed: 12427679]

Manger PR, Restrepo CE, Innocenti GM. The superior colliculus of the ferret: cortical afferents and efferent connections to dorsal thalamus. Brain research. 2010; 1353:74–85. [PubMed: 20682301]

Marion R, Li K, Purushothaman G, Jiang Y, Casagrande VA. Morphological and neurochemical comparisons between pulvinar and V1 projections to V2. The Journal of comparative neurology. 2013; 521:813–832. [PubMed: 22826174]

Ogren MP, Hendrickson AE. The distribution of pulvinar terminals in visual areas 17 and 18 of the monkey. Brain research. 1977; 137:343–350. [PubMed: 412565]

Pallas SL, Roe AW, Sur M. Visual projections induced into the auditory pathway of ferrets. I. Novel inputs to primary auditory cortex (AI) from the LP/pulvinar complex and the topography of the MGN-AI projection. The Journal of comparative neurology. 1990; 298:50–68. [PubMed: 1698829]

Patzke N, Innocenti GM, Manger PR. The claustrum of the ferret: afferent and efferent connections to lower and higher order visual cortical areas. Frontiers in systems neuroscience. 2014; 8:31. [PubMed: 24616671]

Pettersen KH, Hagen E, Einevoll GT. Estimation of population firing rates and current source densities from laminar electrode recordings. Journal of computational neuroscience. 2008; 24:291–313. [PubMed: 17926125]

Poulet JF, Petersen CC. Internal brain state regulates membrane potential synchrony in barrel cortex of behaving mice. Nature. 2008; 454:881–885. [PubMed: 18633351]

Purushothaman G, Marion R, Li K, Casagrande VA. Gating and control of primary visual cortex by pulvinar. Nature neuroscience. 2012; 15:905–912. [PubMed: 22561455]

Raczkowski D, Rosenquist AC. Connections of the multiple visual cortical areas with the lateral posterior-pulvinar complex and adjacent thalamic nuclei in the cat. The Journal of neuroscience : the official journal of the Society for Neuroscience. 1983; 3:1912–1942. [PubMed: 6619917]

Rappelsberger P, Pockberger H, Petsche H. Current source density analysis: methods and application to simultaneously recorded field potentials of the rabbit's visual cortex. Pflugers Archiv : European journal of physiology. 1981; 389:159–170. [PubMed: 6259585]

Rinne P, Hassan M, Goniotakis D, Chohan K, Sharma P, Langdon D, Soto D, Bentley P. Triple dissociation of attention networks in stroke according to lesion location. Neurology. 2013; 81:812–820. [PubMed: 23902704]

Rosenberg DS, Mauguière F, Demarquay G, Ryvlin P, Isnard J, Fischer C, Guénot M, Magnin M. Involvement of medial pulvinar thalamic nucleus in human temporal lobe seizures. Epilepsia. 2006; 47:98–107. [PubMed: 16417537]

Rubinov M, Sporns O. Complex network measures of brain connectivity: uses and interpretations. NeuroImage. 2010; 52:1059–1069. [PubMed: 19819337]

Saalmann YB, Kastner S. Cognitive and perceptual functions of the visual thalamus. Neuron. 2011; 71:209–223. [PubMed: 21791281]

Saalmann YB, Pinsk MA, Wang L, Li X, Kastner S. The pulvinar regulates information transmission between cortical areas based on attention demands. Science. 2012; 337:753–756. [PubMed: 22879517]

Author Manuscript Author Manuscript Author Manuscript Author Manuscript

Schiller PH, Malpeli JG. The effect of striate cortex cooling on area 18 cells in the monkey. Brain research. 1977; 126:366–369. [PubMed: 405082]

Segraves MA, Rosenquist AC. The afferent and efferent callosal connections of retinotopically defined areas in cat cortex. The Journal of neuroscience : the official journal of the Society for Neuroscience. 1982; 2:1090–1107. [PubMed: 6180150]

Sellers KK, Bennett DV, Hutt A, Frohlich F. Anesthesia differentially modulates spontaneous network dynamics by cortical area and layer. J Neurophysiol. 2013; 110:2739–2751. [PubMed: 24047911]

Sellers KK, Bennett DV, Hutt A, Williams JH, Frohlich F. Awake versus Anesthetized: Layer-Specific Sensory Processing in Visual Cortex and Functional Connectivity between Cortical Areas. J Neurophysiol. 2015 jn 00923 02014.

Sherman SM. The thalamus is more than just a relay. Current opinion in neurobiology. 2007; 17:417–422. [PubMed: 17707635]

Sherman SM. Thalamocortical interactions. Curr Opin Neurobiol. 2012; 22:575–579. [PubMed: 22498715]

Sherman SM, Guillery RW. The role of the thalamus in the flow of information to the cortex. Philos Trans R Soc Lond B Biol Sci. 2002; 357:1695–1708. [PubMed: 12626004]

Simoncelli EP, Olshausen BA. Natural image statistics and neural representation. Annual review of neuroscience. 2001; 24:1193–1216.

Snow JC, Allen HA, Rafal RD, Humphreys GW. Impaired attentional selection following lesions to human pulvinar: evidence for homology between human and monkey. Proceedings of the National Academy of Sciences of the United States of America. 2009; 106:4054–4059. [PubMed: 19237580]

Theyel BB, Llano DA, Sherman SM. The corticothalamocortical circuit drives higher-order cortex in the mouse. Nature neuroscience. 2010; 13:84–88. [PubMed: 19966840]

Ulbert I, Halgren E, Heit G, Karmos G. Multiple microelectrode-recording system for human intracortical applications. Journal of neuroscience methods. 2001; 106:69–79. [PubMed: 11248342]

Updyke BV. Projections from visual areas of the middle suprasylvian sulcus onto the lateral posterior complex and adjacent thalamic nuclei in cat. The Journal of comparative neurology. 1981; 201:477–506. [PubMed: 7287931]

Vazquez-Garcia M, Wallman MJ, Timofeev I. Somatotopic organization of ferret thalamus. Frontiers in integrative neuroscience. 2014; 8:90. [PubMed: 25484859]

Vincent JL, Patel GH, Fox MD, Snyder AZ, Baker JT, Van Essen DC, Zempel JM, Snyder LH, Corbetta M, Raichle ME. Intrinsic functional architecture in the anaesthetized monkey brain. Nature. 2007; 447:83–86. [PubMed: 17476267]

Wang L, Saalmann YB, Pinsk MA, Arcaro MJ, Kastner S. Electrophysiological low-frequency coherence and cross-frequency coupling contribute to BOLD connectivity. Neuron. 2012; 76:1010–1020. [PubMed: 23217748]

Wiser AK, Callaway EM. Contributions of individual layer 6 pyramidal neurons to local circuitry in macaque primary visual cortex. The Journal of neuroscience : the official journal of the Society for Neuroscience. 1996; 16:2724–2739. [PubMed: 8786448]

Wong-Riley M. Changes in the visual system of monocularly sutured or enucleated cats demonstrable with cytochrome oxidase histochemistry. Brain research. 1979; 171:11–28. [PubMed: 223730]

Zhang J, Chu KW, Teague EB, Newmark RE, Buchsbaum MS. fMRI assessment of thalamocortical connectivity during attentional performance. Magnetic resonance imaging. 2013; 31:1112–1118. [PubMed: 23727467]

Author Manuscript Author Manuscript Author Manuscript Author Manuscript

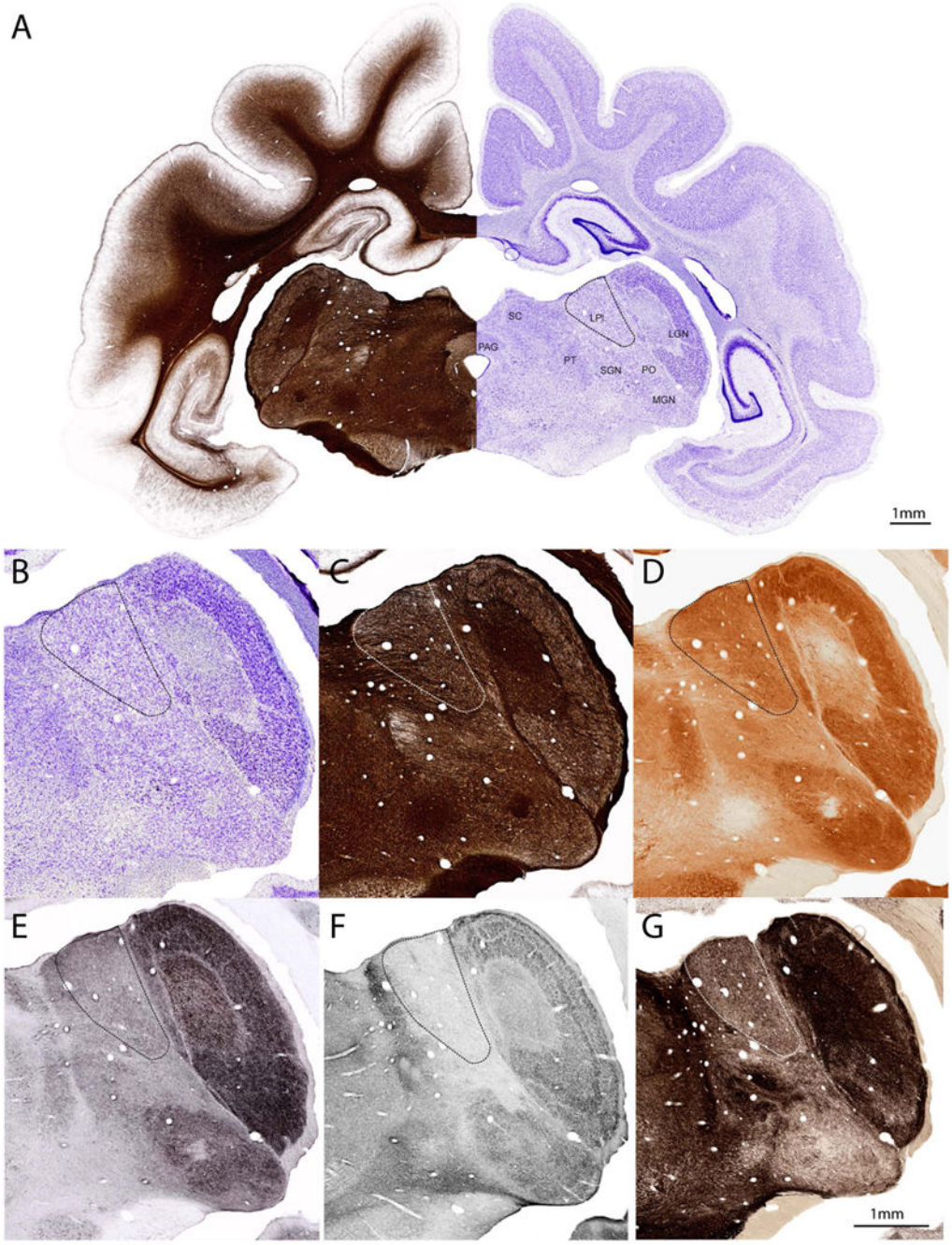

Figure 1.

Six stains of neighboring 50 μm thick sections at the rostrocaudal level of the caudal LPl. **A**, Composite image of a fiber stained (myelin silver impregnation, Gallyas) and a mirrored neighboring section stained for cells (Nissl). Enlarged sections for **B**, Nissl **C,** Fiber **D**, Cytochrome-oxidase. **E**, Parvalbumin. **F**, VGluT2. **G**, AChE. LGN – lateral geniculate nucleus; LPl – lateral LP; MGN – medial geniculate nucleus; PAG – periaqueductal grey; PO – nucleus of the posterior group; PT – pretectal nucleus; SC – superior colliculus; SGN – suprageniculate nucleus.

Author Manuscript Author Manuscript Author Manuscript Author Manuscript

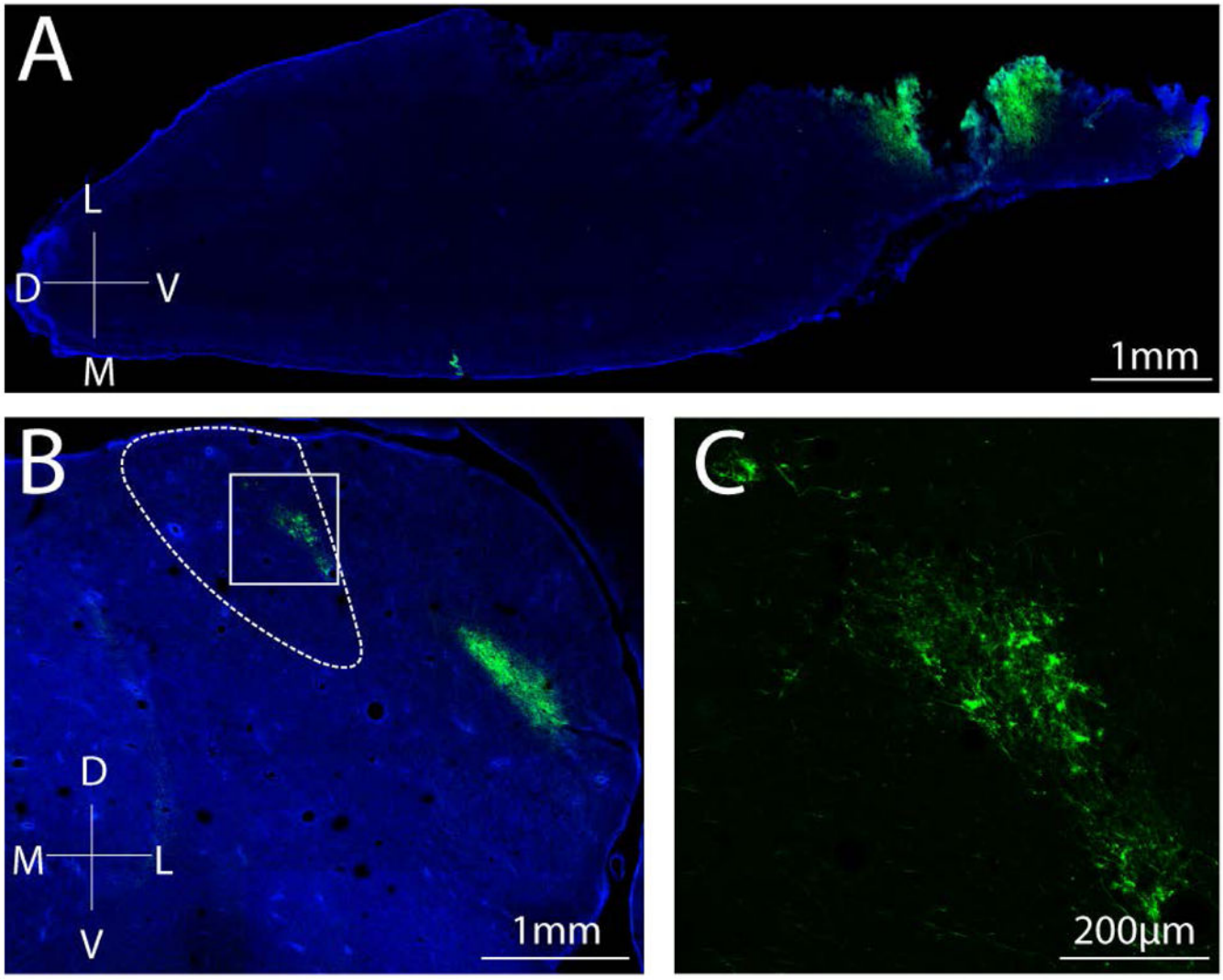

Figure 2.

Anterograde tracer injection shows that area 17 (V1) projects to LPl. **A**, Focal injection site of rAA5-CaMKIIa-ArchT-GFP (green) in the most caudal part of area 17 which covers the whole cortical surface of the forebrain hemisphere at that posterior level. **B**, Restricted anterograde label in caudal LPl (dashed outlined) and LGN. White square: location of panel **C**. **C**, Labeled terminals in LPl. All sections were counterstained with DAPI.

Author Manuscript Author Manuscript Author Manuscript Author Manuscript

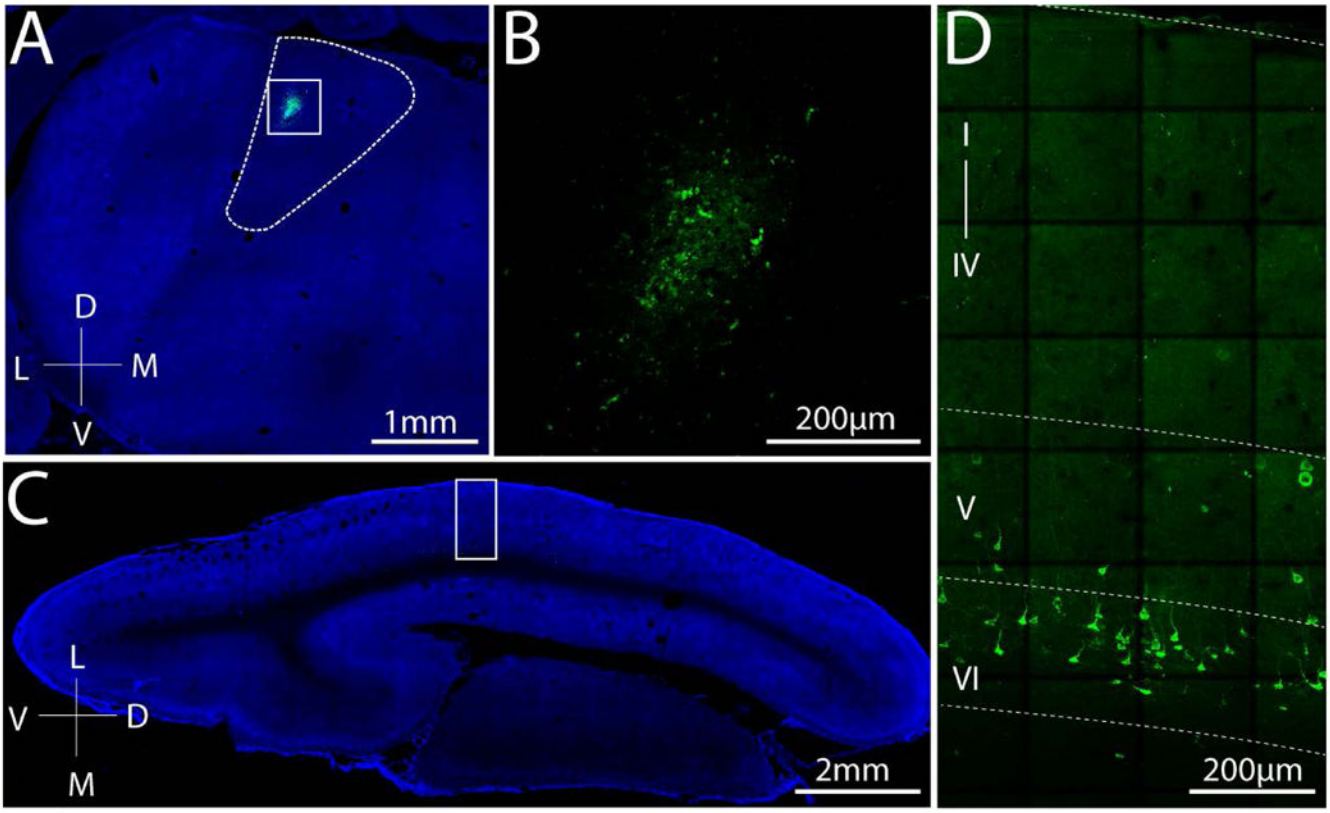

Figure 3.

Retrograde tracer injection established layer specific origin of fibers from area 17 (V1) that project to LPl. **A**, Focal injection site of CTB (green) in LPl. **B**, Enlarged area from **A** (white square). **C,** Retrograde labeling of pyramidal cells in layer V/VI are seen in the more anterior part of area 17. White square: location of enlargement shown in **D** confocal image. **D**, CTB label (488) only. All sections were counterstained with DAPI. Dashed lines indicate the layer boundaries.

Author Manuscript Author Manuscript Author Manuscript Author Manuscript

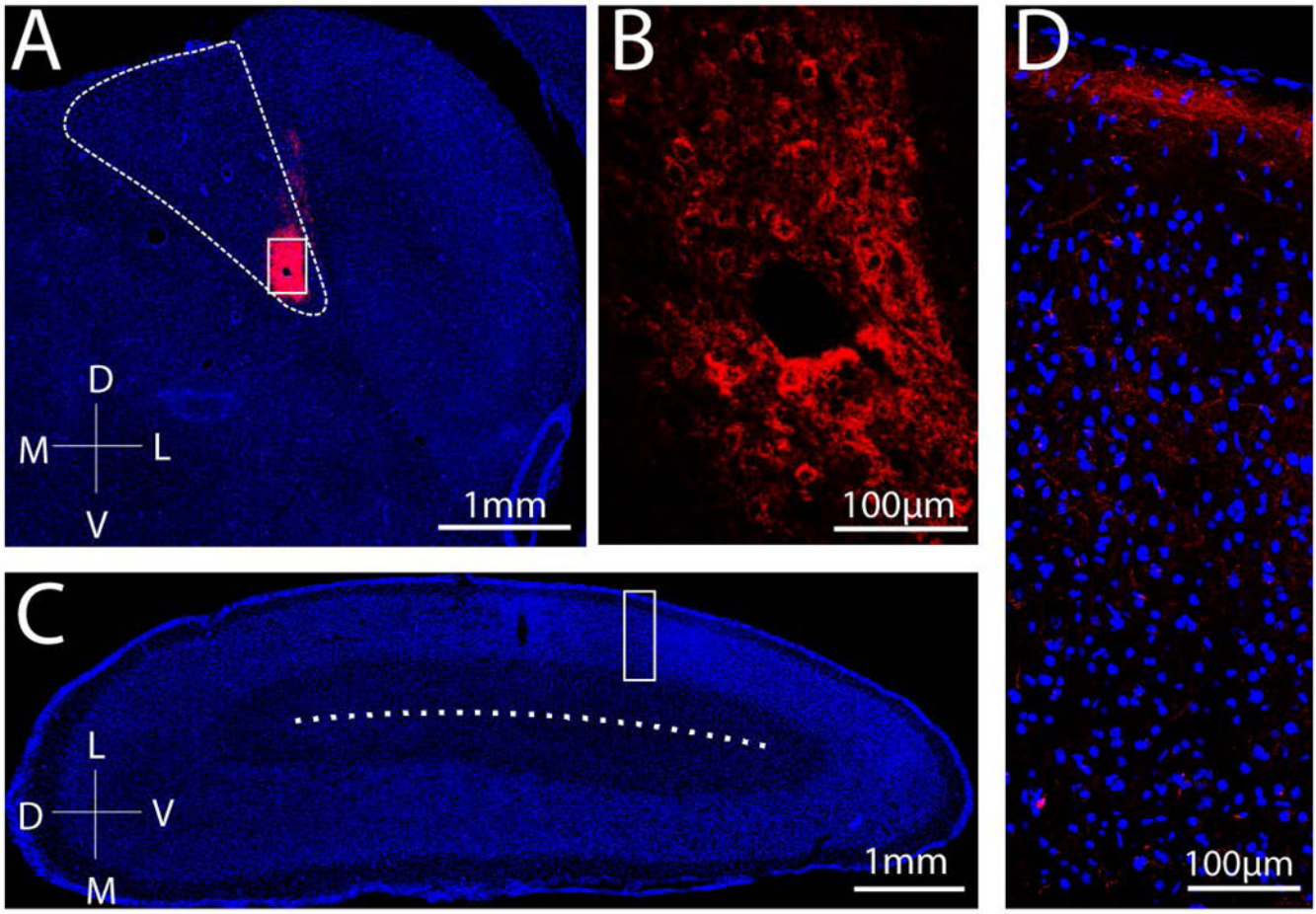

Figure 4.

Anterograde tracer injection delineated target layers of fibers from LPl in area 17 (V1). **A**, Focal injection site of rAAV5-CaMKIIa-ChR-YFPmcherry (red) in the caudal LPl (outlined). White square: location of panel **B**. **B**, Labeled cell bodies in LPl. **C**, Most caudal part of V1 which covers the whole cortical surface of the forebrain hemisphere at that posterior level. Dashed line indicates the location of the almost non-existing underlying white matter at that posterior level. The white square marks the location of the enlargement in **D**. **D**, Dense anterograde label in V1, predominantly in layer I together with the DAPI stained cell nuclei in a confocal image. All sections were counterstained with DAPI.

Author Manuscript Author Manuscript Author Manuscript Author Manuscript

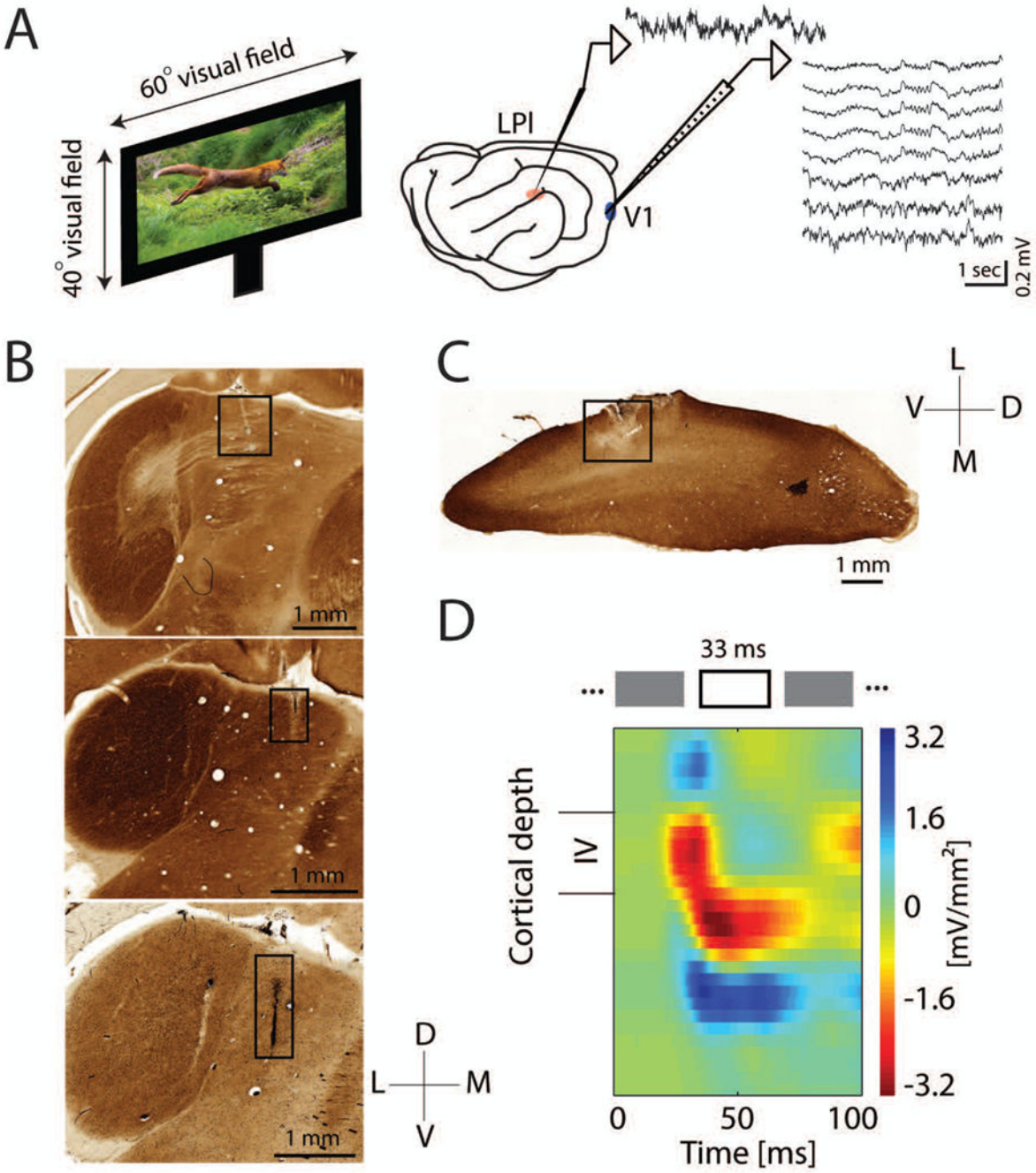

Figure 5.

Design of electrophysiological recording study and identification of cortical layers. **A,** Recording design. Multiunit activity (MUA) and local field potential (LFP) were recorded simultaneously from left LPl (red) and left V1 (blue) during spontaneous activity and visual stimulation. A single metal electrode was used in LPl and a linear probe with 32 channels was used to simultaneously record from all cortical layers (sample raw LFP traces shown). Image shown is similar to original, copyright protected movie clips from BBC, Planet Earth **B**, Three CO-stained coronal sections with the electrode tracks and electrolytic lesions in the

Author Manuscript Author Manuscript Author Manuscript Author Manuscript

lateral region of LPl (representative sections from three ferrets); **C**, CO-stained cortical section with the track of the linear silicon probe in V1. **D**, Top: Stimulus design. Full-field white flashes were presented for 33 msec at a frequency of 1 Hz; Bottom: Cortical layers were identified with CSD analysis by visual stimulation with full-field white flashes. The top of the initial current sink was considered to correspond to the upper edge of layer IV and was used as a point of alignment for all recordings.

Author Manuscript Author Manuscript Author Manuscript Author Manuscript

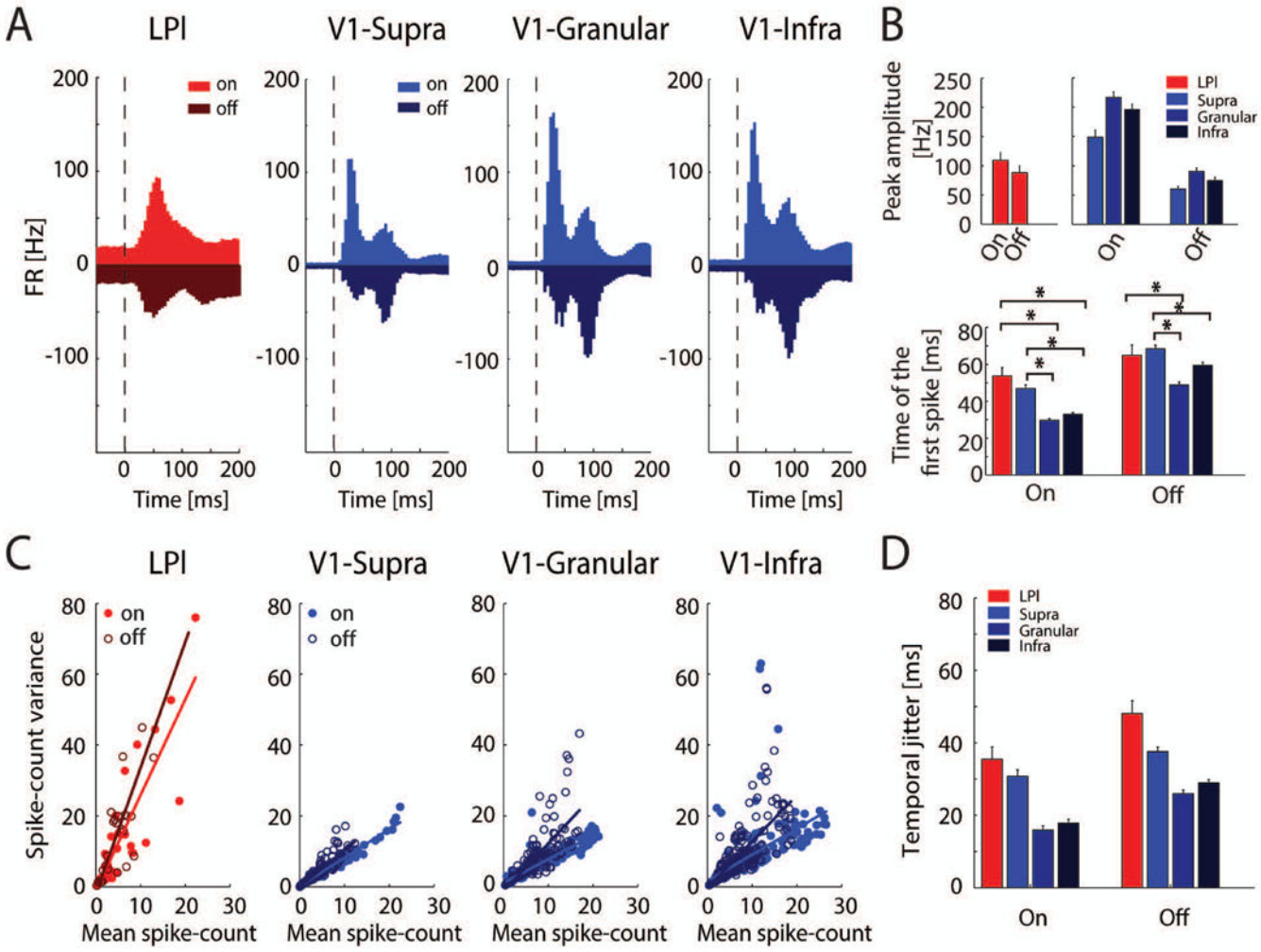

Figure 6.

Visual responses evoked by brief full-field stimulation. **A**, Overall average PSTHs of the MUA in LPl (n=28) and V1 cortical layers during visual stimulation (dashed line: stimulus onset). V1-supra, supragranular (layers 1-2/3, n=173); V1-granular (layer 4, n=151); V1-infra, infragranular (layers 5-6, n=220) ; **B**, Top: Mean peak response amplitude for LPl and V1 layers during white ("on") and black ("off") flashes, measured from the PSTH. Bottom: Mean time to first spike measured from stimulus onset to the first spike for LPl and V1 layers. **C,** Variance of the spike counts as a function of the mean count. Variance increases with the mean, and a steeper slope was found for LP/pulvinar compared to V1 layers. **D**, Spike-timing (temporal) jitter of LPl (n=280 and V1 layers (n=173, 151 and 220) for "on" and "off" responses. Temporal jitter was determined by calculating the standard deviation of the time of the first spike after stimulus onset * indicates $p<0.05$; NS indicates $p>0.05$. Error bars represent standard error of the mean (SEM).

Author Manuscript
Author Manuscript
Author Manuscript
Author Manuscript

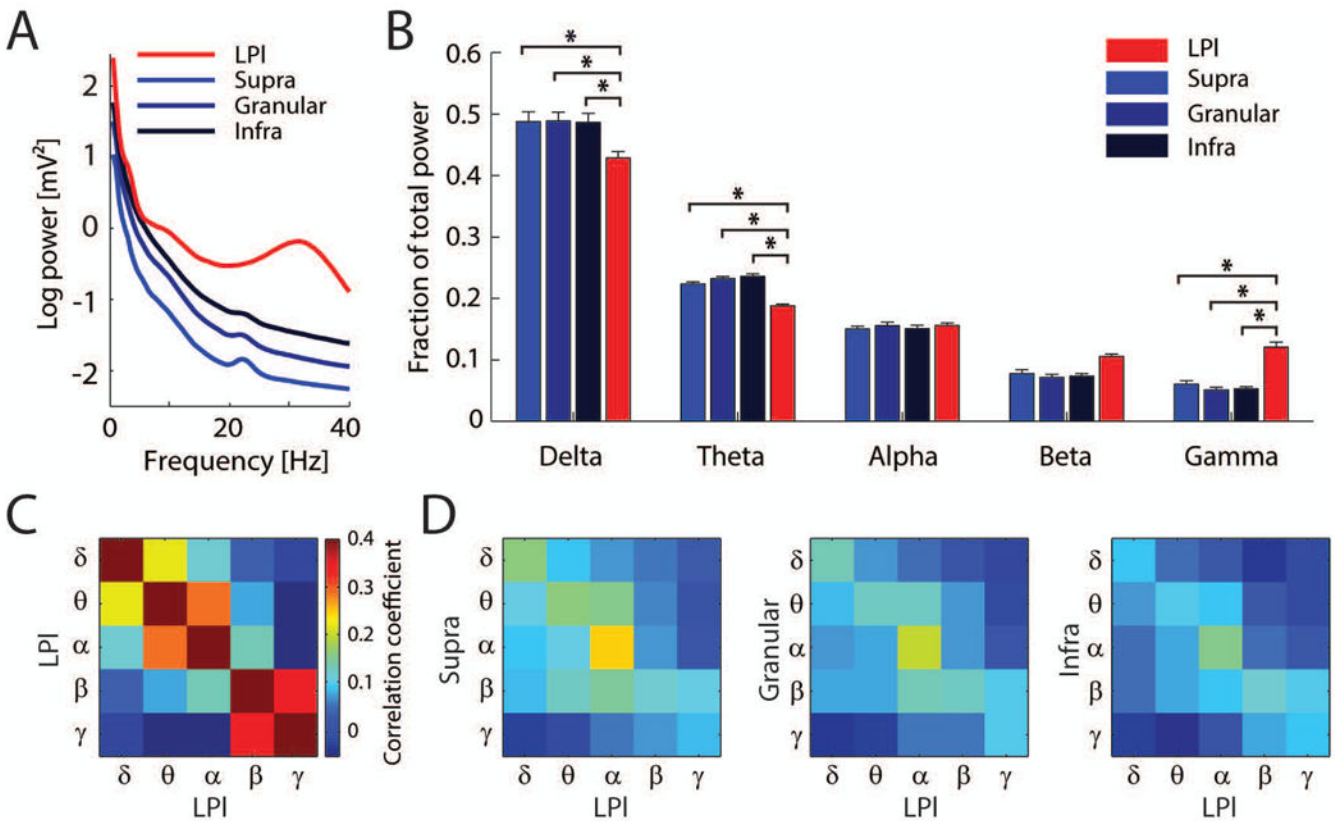

Figure 7.

LFP frequency structure in the LPl and V1 and band-limited LFP power correlations during spontaneous activity **A,** Average LFP power spectra. red: LPl, blue: V1 (shades indicate layers).. **B,** Power in each frequency band as a percentage of total power. Delta, 0.5–4 Hz; theta, 4–8 Hz; alpha, 8–12 Hz; beta, 12–30 Hz; gamma, 30–40 Hz. * indicates $p<0.05$; error bars represent SEM. **C,** Power autocorrelation for LPl. **D,** Power correlation between LPl and V1 layers.

Author Manuscript
Author Manuscript
Author Manuscript
Author Manuscript

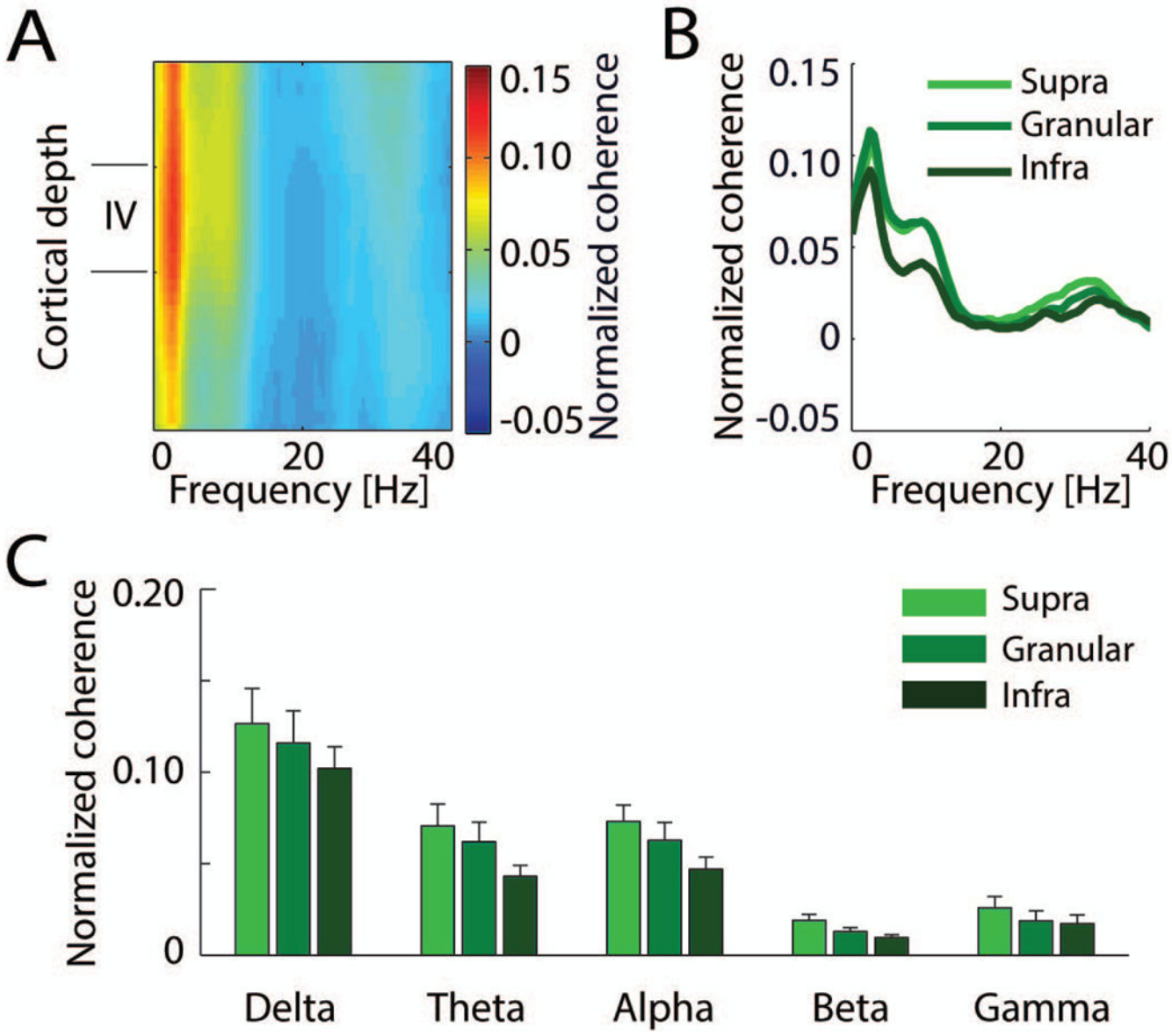

Figure 8.

Layer-dependent coherence between LPl and V1 during spontaneous activity. **A,** Complete coherence depth-profile (coherence as a function of V1 cortical depth). **B,** Normalized coherence between LP/pulvinar and different cortical layers. **C,** Normalized coherence by frequency band and cortical layer. Error bars represent SEM.

Author Manuscript Author Manuscript Author Manuscript Author Manuscript

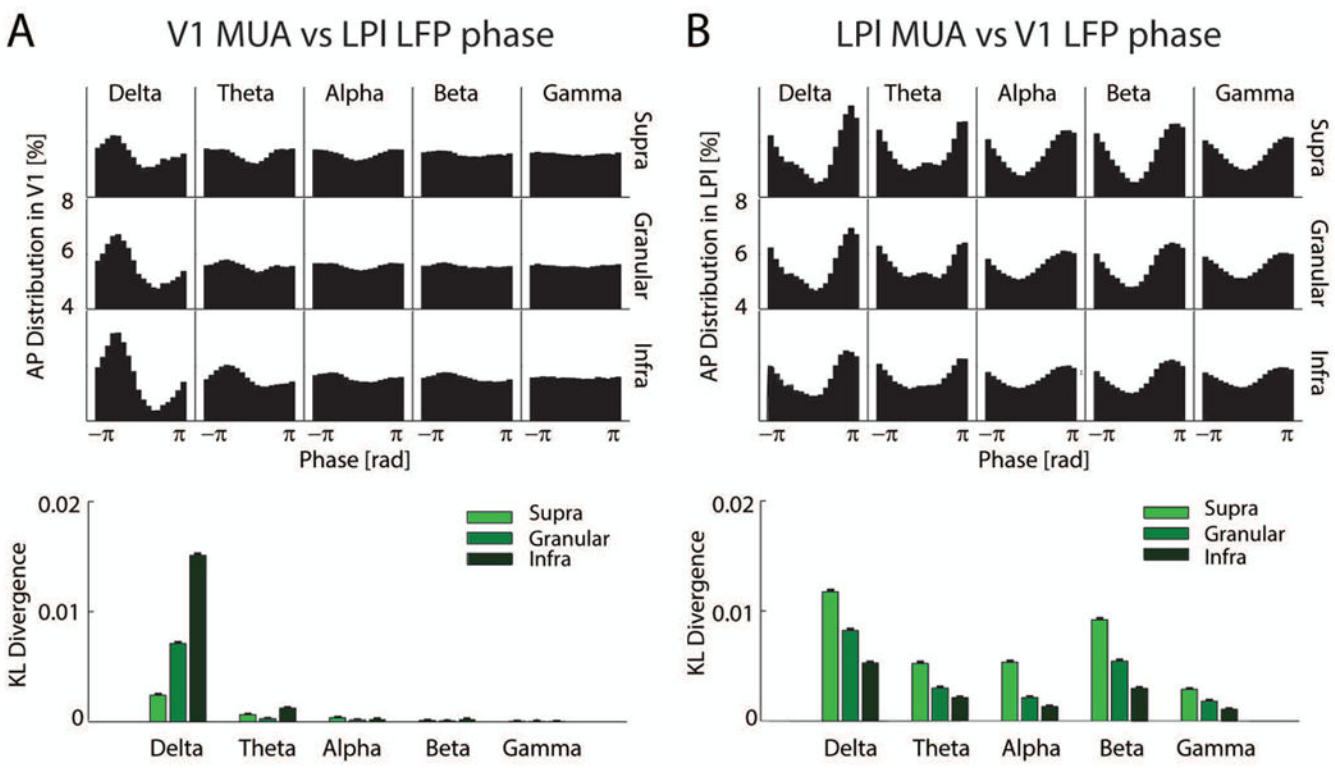

Figure 9.

Spike-phase coupling between LPl and V1 cortical layers (spontaneous activity) **A,** Top: Preferred phase of firing of V1 MU spikes as a function of LPl LFP oscillation phase by cortical layer and frequency band. Bottom: KL Divergence quantifies degree of phase preference. Error bars denote 95% confidence intervals determined by bootstrap. **B**, Top: Phase of LPl MU spikes as a function of V1 LFP oscillation phase by cortical layer and frequency band. Bottom: KL Divergence quantifies degree of phase preference. Error bars as in (**A**).

Author Manuscript Author Manuscript Author Manuscript Author Manuscript

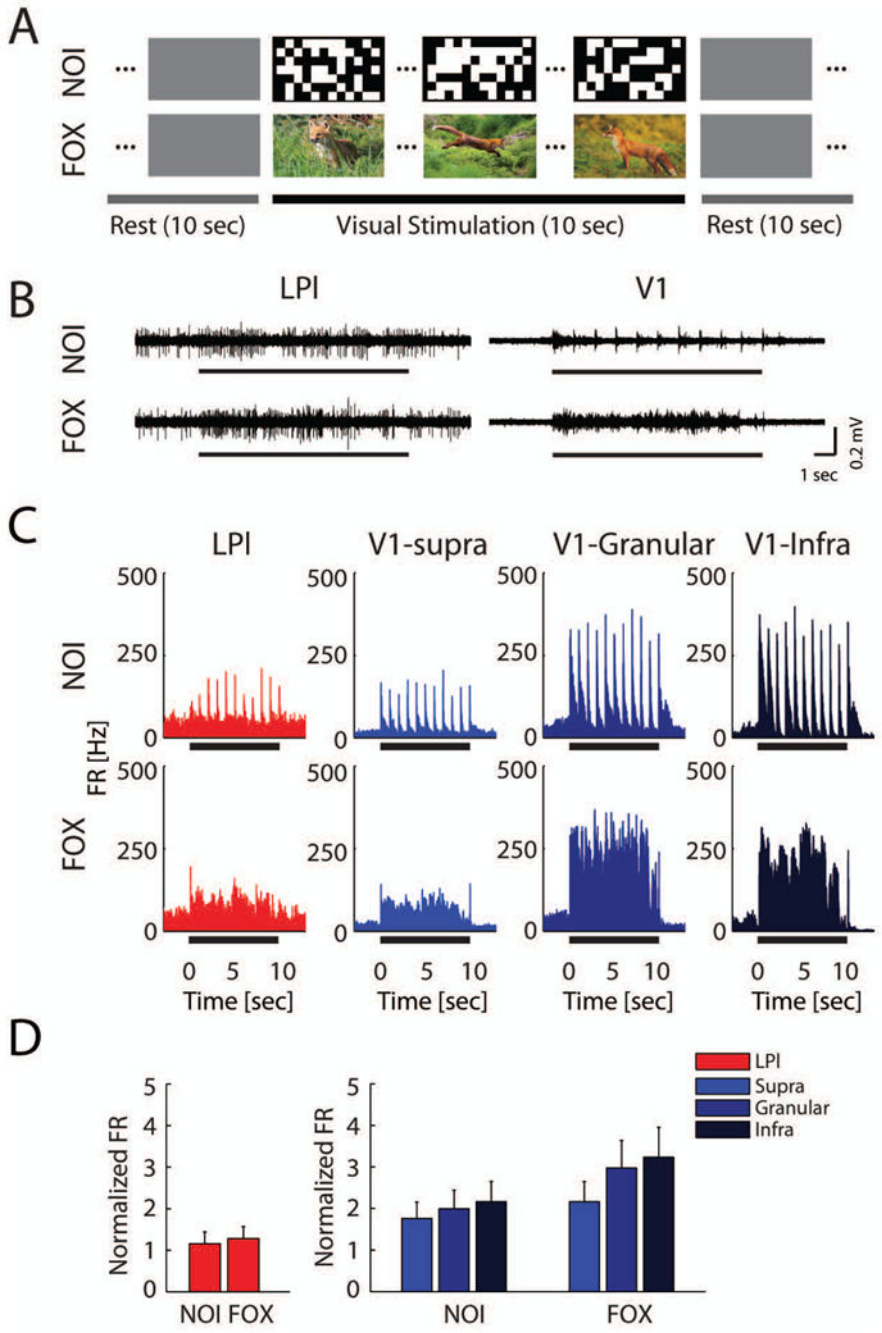

Figure 10.

Visual responses to synthetic and naturalistic stimuli. **A**, Illustration of synthetic and naturalistic visual stimuli. Each trial consisted of ten seconds of visual stimulation bracketed by ten seconds of rest (gray screen). Each stimulus was presented ten times, order randomized. NOI, checkerboard frozen noise stimuli; FOX, naturalistic video clip of foxes (images shown are similar to original, copyright protected movie clips from BBC, Planet Earth). **B**, Representative high-pass filtered raw traces indicate the modulation of LPl (left) and V1 (right) neuronal activity during NOI (top) and FOX (bottom) visual stimuli. Black

lines indicate 10 sec stimulation. **C**, PSTHs of representative MUA in LPl and V1 three layers in response to different types of visual stimuli. **D**, Normalized firing rate of LPl and V1 MUA for different types of visual stimuli. Error bars represents SEM.

Author Manuscript Author Manuscript Author Manuscript Author Manuscript

Author Manuscript Author Manuscript Author Manuscript Author Manuscript

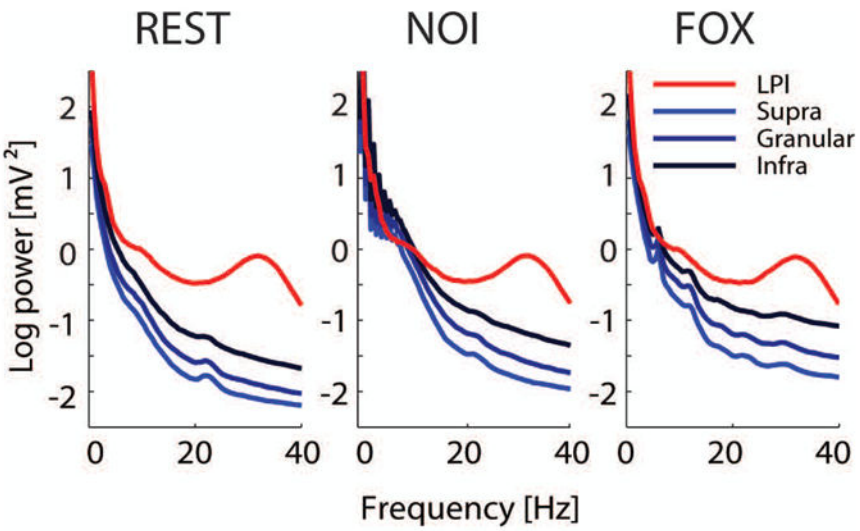

Figure 11.

LFP frequency structure in LPl and V1 layers during visual stimulation. Average LFP power spectra 10 sec before (left) and during the NOI (middle) and FOX (right) stimuli. Red: LPl, Blue: V1 (shades indicate layers).

Author Manuscript Author Manuscript Author Manuscript Author Manuscript

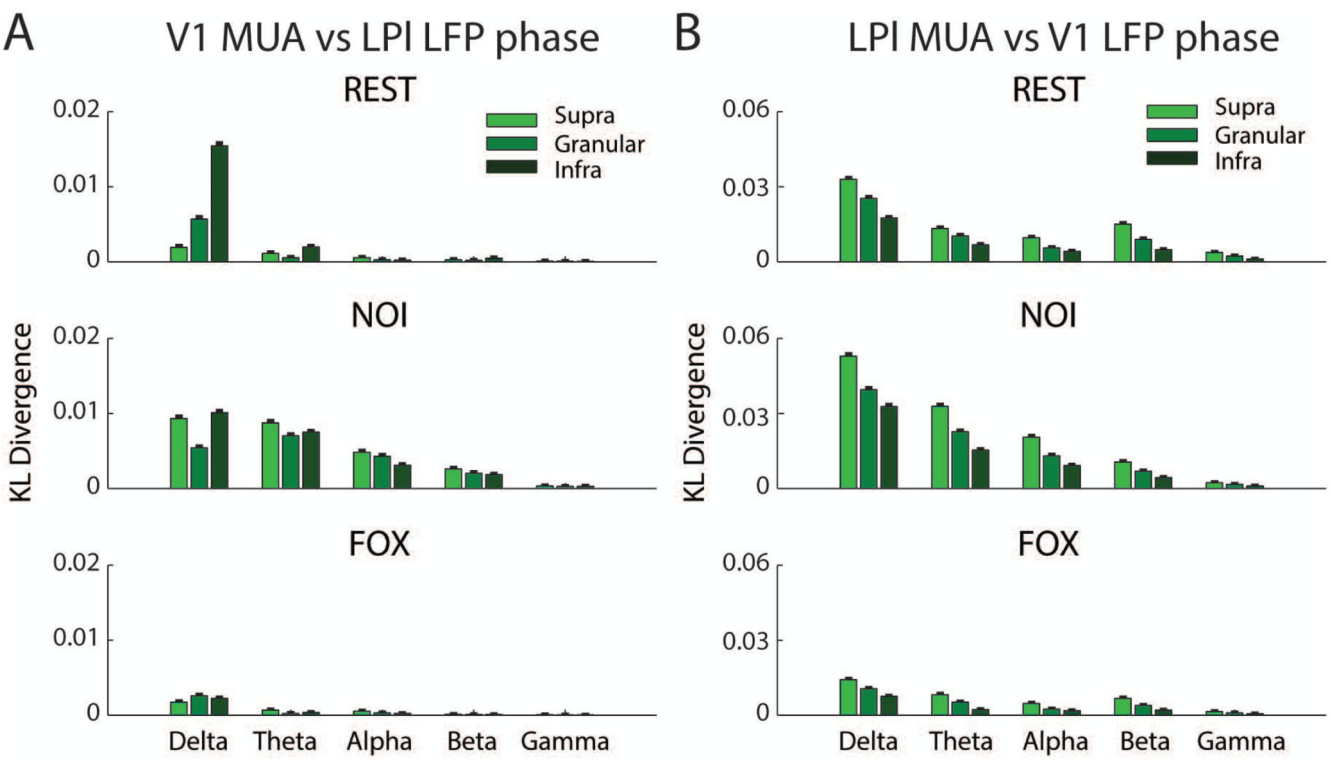

Figure 12.

Spike-phase coupling between LPl and V1 cortical layers during visual stimulation **A,** KL Divergence quantifies degree of phase preference of firing of V1 MU spikes as a function of LPl LFP oscillation phase by cortical layer and frequency band before (REST, top) and during NOI (middle) and FOX (bottom) stimulation. Error bars denote 95% confidence intervals determined by bootstrap. **B**, KL Divergence quantifies degree of phase preference of firing of LPl MU spikes as a function of V1 LFP oscillation phase by cortical layer and frequency band before (REST, top) and during NOI (middle) and FOX (bottom) stimulation. Error bars as in (**A**).